A Solid-State NMR and ab Initio Study of Sodium Metallocenes

Mathew J. Willans and Robert W. Schurko*

Department of Chemistry and Biochemistry, University of Windsor, Windsor, Ontario, Canada N9B 3P4

Received: December 13, 2002; In Final Form: March 5, 2003

Sodium metallocenes (sodocenes) are a fascinating class of molecules that form polymeric chains of repeating $[Cp'Na]_n$ units. A variety of sodium metallocenes have been studied by ^{23}Na ($I = 3/2$) and ^{13}C solid-state NMR, where $Cp' = Cp$ ($C_5H_5^-$), Cp^{Me} ($C_5H_4Me^-$), Cp^{iPr} ($C_5H_4iPr^-$), and Cp* ($C_5Me_5^-$). Simulations of ^{23}Na MAS NMR spectra yield the ^{23}Na quadrupolar coupling constants (C_Q) and asymmetry parameters (η_Q) for all compounds. Values of C_Q range from 2.97 to 3.89 MHz for the linear Cp′Na compounds. A new bent base-substituted species, CpNa·THF (THF = tetrahydrofuran), is identified which has $C_Q = 1.82(2)$ MHz. The sodium nuclei in sodocenes are extremely shielded with respect to the standard sodium chemical shift range, with chemical shifts (δ_{iso}) ranging from −45.5 to −61.9 ppm. All of the linear base-free compounds exhibit values of η_Q near zero, which reflect the axial symmetry of the sodium environments, while the nonlinear CpNa·THF has $\eta_Q = 0.39(2)$, indicative of the electronic asymmetry about the sodium nucleus. Static ^{23}Na NMR experiments reveal subtle instances of ^{23}Na chemical shielding anisotropy, with spans (Ω) ranging from 9.5 to 12.5 ppm. Variable-temperature ^{23}Na NMR experiments show that the magnitude of $C_Q(^{23}Na)$ grows with increasing temperature in the linear metallocenes. Ab initio calculations were performed on a variety of structural models to gain insight into the nature of the electric field gradient (EFG) and chemical shielding (CS) tensors. Rotation of the Cp′ rings and changes in the inter-ring distances were examined in order to see how these motions affect the ^{23}Na EFG tensors. A combination of experimental and theoretical data indicate that inter-ring distances decrease in the linear sodocenes as the samples are heated. Solid-state ^{13}C CPMAS NMR experiments are used to probe the purity and crystallinity of the metallocene samples to confirm the existence of the bent ligated metallocene CpNa·THF and to examine the effect of dynamic ring motion on observed carbon chemical shielding tensors of the Cp′ ring carbons.

Introduction

Metallocenes are organometallic complexes that contain π-bonded five-membered carbon cyclopentadienyl (Cp) ligands and have the general formula Cp'_nM ($Cp' = C_5R_5^-$, R = H, Me, Ph, Bz, etc.; M = metal atom). The pentamethylcyclopentadienyl anion ($Cp^* = C_5Me_5^-$) rivals the cyclopentadienyl anion in its occurrence as a metallocene ligand due to the generally increased solubility and stability observed in compounds when Cp is replaced by Cp*. Asymmetrically substituted Cp′ ligands, $C_5H_mR_{5-m}^-$, where R = Me, *i*Pr, $SiMe_3$, etc., are also common. Main group metallocenes are remarkable in that they have the ability to adopt a wide variety of molecular geometries, have a number of interesting bonding types and hapticities, and form a structurally and chemically diverse group of compounds.[1] An important class of main-group metallocenes are the alkali-metal metallocenes. Such compounds have a long and rich history in chemistry, as CpNa and CpK were among the first prepared and isolated organometallic alkali-metal compounds.[2] Perhaps more importantly, they are among the most commonly used reagents for the synthesis of many other types of metallocenes.

Bonding in these compounds is dominated by electrostatic attraction between the negatively charged Cp′ ring and the positively charged alkali metal. In addition, these compounds tend to form polymeric molecules, commonly referred to as "supersandwiches", composed of repeating $[Cp'M]_n$ units. Such supersandwiches can adopt a linear geometry, where the angle between the centroids of two Cp′ rings and the metal ($Cp'_{cent}-M-Cp'_{cent}$) is close to 180°, or they can adopt a bent geometry, where this angle is generally about (140 ± 10)°. The type of geometry that is adopted depends on both the nature of the Cp′ ligand and the size of the alkali metal (Figure 1). The Cp′ ligands in alkali-metal metallocenes tend to have an η^5 hapticity, where bonding between the Cp′ ring and the metal is evenly distributed between all five carbon atoms in the Cp′ ring.

Limitations in the chemistry and structural characterization of alkali-metal metallocenes lie mostly in the fact that they are insoluble in nonpolar solvents and have relatively poor solubility in polar solvents. Commonly used polar solvents such as THF and TMEDA may act as ligands that bind to the metal cation. As isolated base-free compounds, they tend to form very fine microcrystalline powders. In addition, these compounds are almost universally sensitive to exposure to both air and moisture. As a result, many single-crystal structure determinations have been on species containing solvent molecules as ligands. Some known exceptions are $K[C_5H_4(SiMe_3)]$, $Li[C_5H_4(SiMe_3)]$ and $K[C_5H_2(SiMe_3)_3-1,2,4]$.[3−5]

Only recently, with X-ray powder diffraction techniques and utilization of the Rietveld method,[6,7] have several base-free alkali-metal metallocenes been structurally characterized. Examples include CpLi, CpNa, CpK,[8] CpRb,[9] CpCs,[10] Cp*Li,[11] and Cp*Na.[12] CpNa and Cp*Na both form essentially linear polymers with $Cp'_{cent}-Na-Cp'_{cent}$ angles of 177.7° and 177.3°, respectively (Figure 2a). In CpNa, the coplanar Cp rings adopt an eclipsed conformation (Figure 2b), whereas the Cp*Na

* To whom correspondence should be addressed. E-mail: rschurko@uwindsor.ca, web: http://www.uwindsor.ca/schurko.

10.1021/jp022590o CCC: $25.00 © 2003 American Chemical Society
Published on Web 05/10/2003

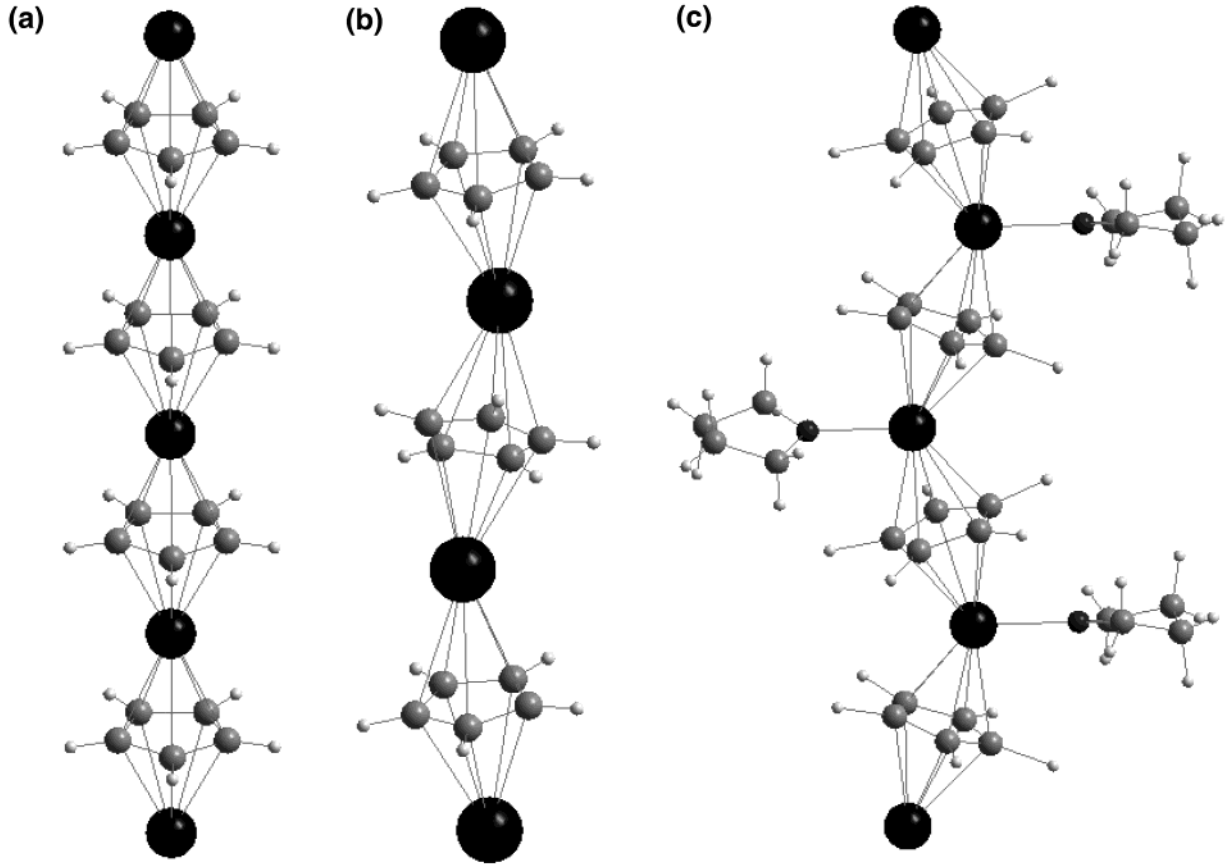

Figure 1. Crystal structures of various alkali-metal metallocenes (a) CpLi, CpNa; (b) CpK, CpCs; and (c) CpNa·THF (proposed structure).

complex has both an eclipsed and slightly staggered Cp* ring conformation (the rings are staggered by a dihedral angle of 13.89° in the latter case, Figure 2c). The Cp'_{cent}−Na distance decreases from 2.357 Å for CpNa to 2.3057 Å for Cp*Na. This shortening is attributed to the stronger electron-donating character of the Cp* ligand in comparison to that of the Cp ligand (the same trend is observed for CpLi and Cp*Li).[5]

Due to the inability of base-free alkali-metal metallocenes to readily form large single crystals, solid-state NMR should prove to be a very useful technique for probing the structure of these substances. Solid-state NMR can provide detailed information on the chemistry, structure and dynamics of metallocenes by either acquiring NMR spectra of the central metal nucleus or probing the rings directly with ^{13}C and ^{1}H NMR experiments. The relatively few studies that focus on NMR of the central metal nuclei include ^{119}Sn and ^{207}Pb studies of stannocenes and plumbocenes,[13−15] a ^{171}Yb CPMAS NMR study of $Cp'_2Yb(II)$ complexes[16] and a single-crystal ^{59}Co study of $[Cp_2Co]NO_3 \cdot H_2O$.[17] Only two such studies have been reported for alkali-metal metallocenes: a ^{7}Li study of lithocenes and related complexes[18] and a brief communication discussing solid-state ^{23}Na NMR of CpNa-TMEDA.[19] Our research group has recently started to examine the relationships between the anisotropic NMR interaction tensors of half-integer quadrupolar nuclei and the structures of main group metallocenes, including a ^{27}Al and ^{13}C NMR study of the decamethylaluminocenium cation[20] and a $^{11}B/^{13}C/^{1}H$ NMR study of boron metallocenes.[21]

Sodocenes are ideal systems to study via solid-state NMR, since ^{23}Na is a very good NMR nucleus due to its 100% natural abundance and relatively large magnetogyric ratio that is similar to that of ^{13}C. ^{23}Na is a quadrupolar nucleus with spin 3/2 and has a moderately sized nuclear quadrupole moment ($Q = 1.0 \times 10^{-29}$ m^2).[22] The ^{23}Na quadrupolar coupling constant (C_Q) values range from about 0.3 MHz for sodium atoms in environments of high spherical symmetry up to 11.34 MHz for Na_3OCl.[23] In solution, ^{23}Na chemical shifts range from −70 to 20 ppm, although anything less than −30 ppm is quite uncommon.[24] In solids, the typical sodium chemical shift range for diamagnetic compounds is from −30 to 25 ppm. The largest reported shifts range from −61.9 ppm for NaV_6O_{15}[25] to 55.1 ppm for Na_2O.[23] Thus, in solids, the observed values of $C_Q(^{23}Na)$ and η_Q may be more useful in elucidating metallocene chemistry and molecular structure than the ^{23}Na chemical shift.

In this paper we report a solid-state magic-angle spinning (MAS), variable-temperature (VT) MAS and static (stationary sample) ^{23}Na NMR study of a variety of sodocenes, including CpNa, Cp*Na, $Cp^{Me}Na$ ($Cp^{Me} = C_5H_4Me^-$) and $Cp^{iPr}Na$ ($Cp^{iPr} = C_5H_4iPr^-$). We also identify the ligated CpNa·THF species obtained from a rapid recrystallization of pure CpNa from THF. Simulations of ^{23}Na MAS NMR spectra are used to extract quadrupolar parameters and chemical shifts. The sensitivity of the C_Q to changes in the molecular structure is probed. Dynamics of the Cp′ rings are probed via variable-temperature ^{23}Na and ^{13}C NMR experiments. Examples of small sodium chemical shielding anisotropy (CSA) in these molecules are revealed from static NMR experiments. Ab initio RHF and hybrid-DFT (B3LYP) calculations were performed to gain further insight into the nature of the sodium electric field gradient (EFG) tensor and sodocene molecular dynamics.

This research serves multiple purposes: First, it is demonstrated that ^{23}Na and ^{13}C solid-state NMR experiments provide an efficient and accurate means of structurally characterizing and differentiating these polycrystalline, polymeric materials. Such experiments also provide a rapid means of determining the purity of these insoluble materials, which are often difficult to synthesize and purify. Second, on a fundamental level, the

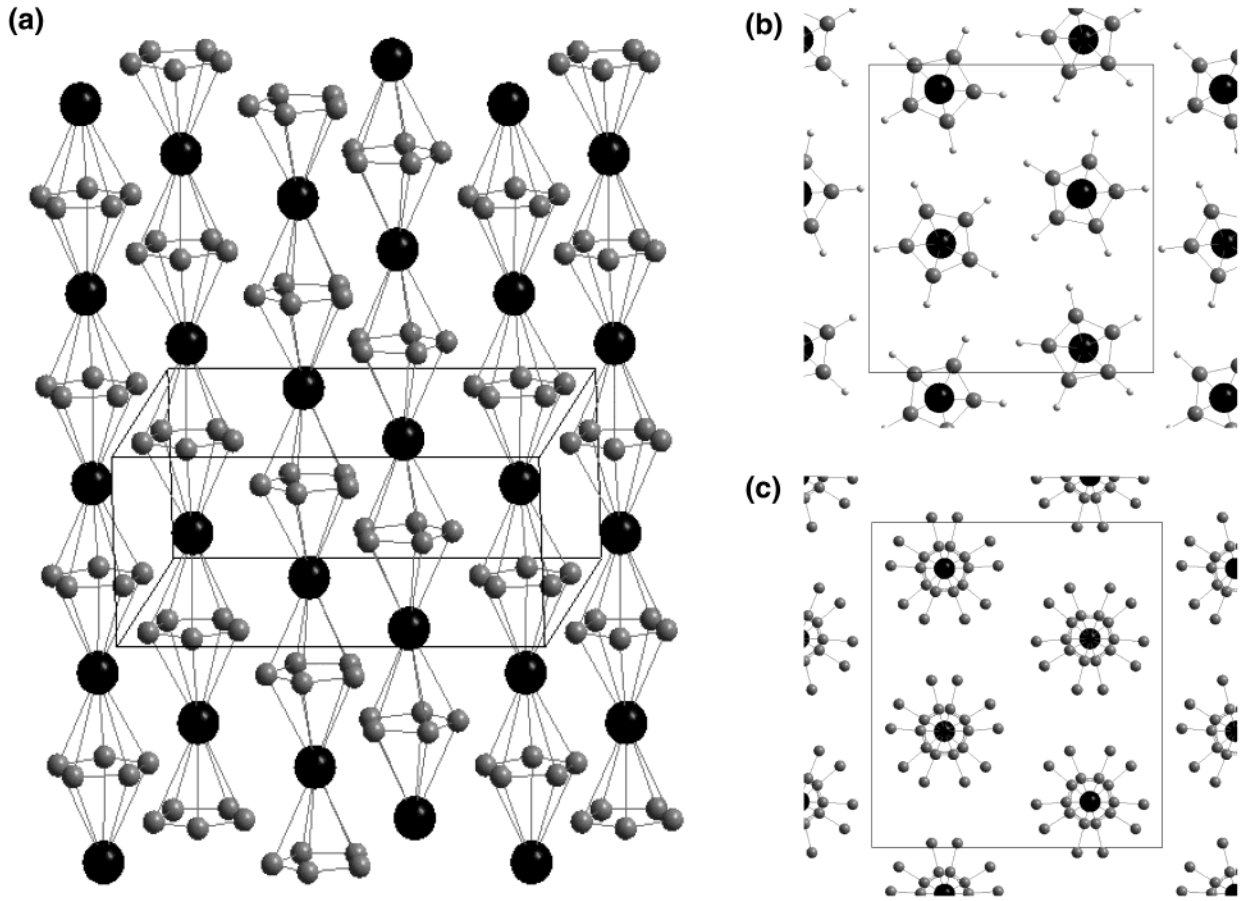

Figure 2. Unit cell of (a) CpNa, view along the *a*-axis (protons omitted for clarity); (b) CpNa, view along the *c*-axis; and (c) Cp*Na, view along the *a*-axis; showing the staggered conformation.

origins of anisotropic NMR interactions are probed by experiment and theory in these chemically and structurally tuneable molecules. Third, we demonstrate that straightforward relationships can be found to exist between the magnitude and symmetry of anisotropic NMR interaction tensors and the chemistry of complicated materials at the molecular level. An understanding of such fundamental relationships provides a basis for using solid-state NMR to study systems of unknown composition and structure and to relate the molecular structure to the bulk properties of the material.

Theoretical Background. The theory behind the simulation of NMR spectra in the high-field approximation using analytical expressions is well summarized elsewhere.[26] In this section, we simply define the NMR interaction tensors and associated parameters.

Both the chemical shielding and quadrupolar interactions are described by second-rank tensors, denoted $\bar{\sigma}$ and $\bar{\mathbf{V}}$, respectively. The chemical shielding (CS) tensor, $\bar{\sigma}$, describes the anisotropic magnetic shielding of a nucleus within a molecule with respect to the bare nucleus, having three principal components in its own principal axis system (PAS) defined from least to most shielded as $\sigma_{11} \leq \sigma_{22} \leq \sigma_{33}$. Only the symmetric portion of the chemical shielding tensor makes observable contributions to NMR spectra. Differences in chemical shielding are typically described with respect to an arbitrary reference compound, such that the chemical shift of a sample, δ_{sample}, is defined as $\delta_{sample} = (\sigma_{ref} - \sigma_{sample})/(1 - \sigma_{ref}) \times 10^6 \approx \sigma_{ref} - \sigma_{sample}$, and the chemical shift tensor is defined such that the principal components are assigned from least to most shielded as $\delta_{11} \geq \delta_{22} \geq \delta_{33}$. The anisotropy of the chemical shift tensor can alternatively be described with three other parameters, δ_{iso}, Ω and κ, which are defined below. Random tumbling of molecules results in averaging of the chemical shift tensor to a single isotropic chemical shift, $\delta_{iso} = (\delta_{11} + \delta_{22} + \delta_{33})/3$, which can easily be measured in liquid or gas phases. The span (Ω) is a measure of the breadth of the chemical shift anisotropy (CSA) and is defined as $\Omega = \delta_{11} - \delta_{33} = \sigma_{33} - \sigma_{11}$. The skew ($\kappa$) is a dimensionless measure of the axial symmetry of the chemical shift tensor and is defined as $\kappa = 3(\delta_{22} - \delta_{iso})/\Omega = 3(\sigma_{iso} - \sigma_{22})/\Omega$, where $-1 \leq \kappa \leq +1$.[27]

The quadrupolar tensor $\bar{\mathbf{Q}}$ is equivalent to $\bar{\mathbf{Q}} = (eQ/2I(2I-1))\bar{\mathbf{V}}$, where $\bar{\mathbf{V}}$ is the EFG tensor. The EFG tensor is traceless and symmetric, and has three principal components defined from smallest to largest as $|V_{11}| \leq |V_{22}| \leq |V_{33}|$. Since $\bar{\mathbf{V}}$ is traceless, the EFG tensor can be completely described by two parameters: the quadrupolar coupling constant C_Q and the quadrupolar asymmetry parameter η_Q. C_Q is a measure of the magnitude of the quadrupolar interaction and is given by $C_Q = eQeq/h = eQV_{33}/h$ where eQ is the nuclear quadrupole moment and $eq = V_{33}$ (the largest component of the EFG tensor). η_Q is a measure of axial symmetry of the EFG tensor and is defined as $\eta_Q = (V_{11} - V_{22})/V_{33}$, where $0 \leq \eta_Q \leq 1$.

Static NMR experiments on half-integer quadrupolar nuclei yield powder patterns which are dependent upon the magnitude and asymmetry of both the anisotropic chemical shielding and the quadrupolar interactions, as well as the relative orientation of these two interactions. The relative orientation of the EFG and CS tensors can be defined by three Euler angles, α, β and γ, which describe counterclockwise rotations of the CS tensor PAS with respect to the EFG PAS about an initial Z axis, a new Y' axis, and finally a new Z'' axis, according to previously described conventions.[26] Thus, to properly simulate a static

NMR powder pattern influenced by both quadrupolar and chemical shielding interactions, one must take into account eight separate parameters: δ_{iso}, Ω, κ, C_Q and η_Q, as well as α, β and γ.[28] Since C_Q, η_Q and δ_{iso} can often be determined from corresponding MAS experiments, the problem can be reduced to five parameters. The relative orientation of the tensors and sometimes even the skew of the chemical shielding tensor can be inferred by the symmetry of the molecule, which in many cases reduces the problem of simulating the spectrum to a single unique solution.

Experimental Section

Synthesis of CpNa. CpNa was synthesized using a slight modification of a literature preparation.[8] Freshly distilled cyclopentadiene was added to a suspension of sodium metal in hexanes and was left to stir overnight. The resulting white-gray mixture was left to settle. The product settled on the top layer, and it was removed, washed with toluene and dried under vacuum. Purity was checked by solution NMR in 99% THF-d_8, using THF-d_8 as an internal reference for ^{1}H and ^{13}C and a 1.0 M NaCl solution as an external reference (0.0 ppm) for ^{23}Na. All spectra agreed with literature values where available. ^{1}H NMR (500.1 MHz) δ 5.64.[29] ^{13}C{^{1}H} NMR (125.8 MHz) δ 103.5.[30] ^{23}Na{^{1}H} NMR (132.3 MHz) δ −33.4. In addition, CpNa was purchased from Aldrich as a 2.0 M solution in THF. The THF was removed in vacuo, and the resulting compound was refluxed in toluene for several hours and dried under vacuum overnight.

Synthesis of Cp^{Me}Na. Cp^{Me}Na was prepared using a slight modification of a literature preparation.[31] Freshly distilled methylcyclopentadiene was added to a suspension of NaH in hexanes and was left to stir overnight. The resulting mixture was filtered and the solid removed. The white product was washed with hexanes and dried under vacuum. ^{1}H NMR (500.1 MHz) δ 5.41 (*o*-$C_5H_4CH_3$), 5.38 (*m*-$C_5H_4CH_3$), 2.13 ($C_5H_4CH_3$).[32] ^{13}C{^{1}H} NMR (125.8 MHz) δ 113.5 (*i*-$C_5H_4CH_3$), 103.9 (*o*-$C_5H_4CH_3$), 102.1 (*m*-$C_5H_4CH_3$), 16.0 ($C_5H_4CH_3$). ^{23}Na{^{1}H} NMR (132.3 MHz) δ −36.5.

Cp^{iPr}Na and Cp*Na. Cp^{iPr}Na was purchased from Strem and used without further purification. Cp*Na was purchased from Aldrich as a 0.5 M solution in THF. Solvent was removed by vacuum, and the base-free, off-white product was isolated.

CpNa·THF. CpNa was purchased from Aldrich as a 2.0 M solution in THF. The solvent was removed gently by vacuum for several hours. An off-white product, which proved to be a mixture of CpNa and CpNa·THF (vide infra), was isolated.

Solid-State NMR. Samples were ground into a fine powder under an inert atmosphere and tightly packed into 4 mm o.d. zirconium oxide rotors, sealed with airtight caps. Solid-state ^{23}Na and ^{13}C NMR spectra were obtained on a Varian Infinity Plus NMR spectrometer at 9.4 T (ν_o(^{23}Na) = 105.74 MHz). A Varian/Chemagnetics 4 mm double-resonance MAS probe, employing high-power CW proton decoupling during acquisition, was used for all ^{23}Na and ^{13}C NMR experiments, with typical decoupling fields ranging from 50 to 65 kHz.

Sodium chemical shifts were referenced to a 1.0 M solution of NaCl (δ_{iso} = 0.0 ppm). For all ^{23}Na experiments, the pulse delays were calibrated and ranged from 4.0 s for singly substituted compounds to 6.0 s for Cp*Na. Hahn-echo static experiments were performed using central-transition selective pulse widths ranging from 1.45 to 17.5 μs and rf fields of 7.14 to 86.2 kHz. The number of scans ranged from 64 to 4000, and the interpulse delay ranged from 80 to 200 μs. All MAS experiments were performed with a 14 kHz rotor speed, the number of scans ranging from 100 to 400. Bloch decay MAS experiments with an rf strength of 33.3 kHz and a 3.5 μs selective pulse width were performed for all singly substituted compounds. The ^{23}Na MAS NMR spectrum of Cp*Na was obtained using a rotor-synchronized Hahn-echo experiment (one rotor-period) with a pulse width of 1.45 μs and ν_1 = 86.2 kHz. Variable-temperature NMR experiments were performed with a decreased number of scans, ranging from 44 to 96, at temperatures ranging from −140 to 125 °C. Temperatures were measured with a thermocouple external to the sample and are not calibrated, though temperature differentials of less than 5 °C are expected at the extreme temperature limits (i.e., −140 °C). Variable-temperature experiments were performed at slower spinning speeds ranging from 8.0 to 9.5 kHz. A decreased rf strength of 26.3 kHz and increased pulse width of 4.5 μs were utilized in some cases.

Carbon-13 NMR spectra were referenced to TMS (δ_{iso}(^{13}C) = 0.0 ppm) by setting the high-frequency resonance of adamantane to 38.57 ppm. All CPMAS and variable-amplitude (VA) CPMAS experiments were conducted with an rf field of 62.5 kHz and pulse widths ranging from 3.5 to 4.0 μs. Samples were spun at various speeds, ranging from 2 to 6 kHz, which were carefully selected to prevent overlap of isotropic peaks and spinning sidebands. The number of transients collected varied from 100 to 200. All experiments employed pulse delays of 9−10 s and optimized contact times of 12−15 ms.

Spectral Simulations. Analytical simulations of the ^{23}Na NMR spectra were performed on a Pentium III computer using the WSOLIDS simulation package. This package was developed by Dr. Klaus Eichele in Prof. Wasylishen's laboratory at Dalhousie University. WSOLIDS incorporates the space-tiling method of Alderman and co-workers for the generation of frequency domain solid-state NMR powder patterns.[33] For simulations of ^{23}Na MAS NMR spectra, spinning sidebands were summed into the central isotropic sideband to simulate the fast-spinning limit. Simulation of ^{13}C powder patterns affected by molecular motion were simulated using a custom-written C++ chemical exchange program. Calculations were carried out on a Dell Precision 420 dual-733 MHz Parallel Pentium III computer. Hemispherical ZCW angle sets were used for powder averaging,[34] and inversion and diagonalization routines for square matrices were performed with release 3.0 of the LAPACK linear algebra package.[35]

Theoretical Methods. Ab initio calculations were conducted using the Gaussian 98 program suite[36] on a Dell Precision 420 dual-733 MHz Pentium III computer. EFG and CS tensors were calculated using RHF and B3LYP (Becke's three-parameter hybrid[37] and correlation functional of Lee, Yang and Parr[38]) methods and the 6-31G** and 6-311G** basis sets. Calculations were performed on clusters constructed from previously determined crystal structures of CpNa[8] and Cp*Na,[12] using various cluster sizes (see Results and Discussion for details). Methyl protons were added to Cp*Na using MOLDEN and their positions optimized at the B3LYP/6-31G** level. Calculations on CpNa·THF clusters were performed on a geometry-optimized structure at the B3LYP/6-31G** level, due to the unavailability of a crystal structure. Z-matrices, in which changes in the Cp'_{cent}−Na distances and rotation of the Cp′ rings could be easily made, were constructed on the basis of the parameters of the crystal structures of CpNa and Cp*Na and the geometry-optimized structure of CpNa·THF.

Embedded cluster calculations[39] were performed on different CpNa clusters at all levels of theory. The lattice was chosen to be a 20 Å sphere consisting of 1999 atoms, originating from

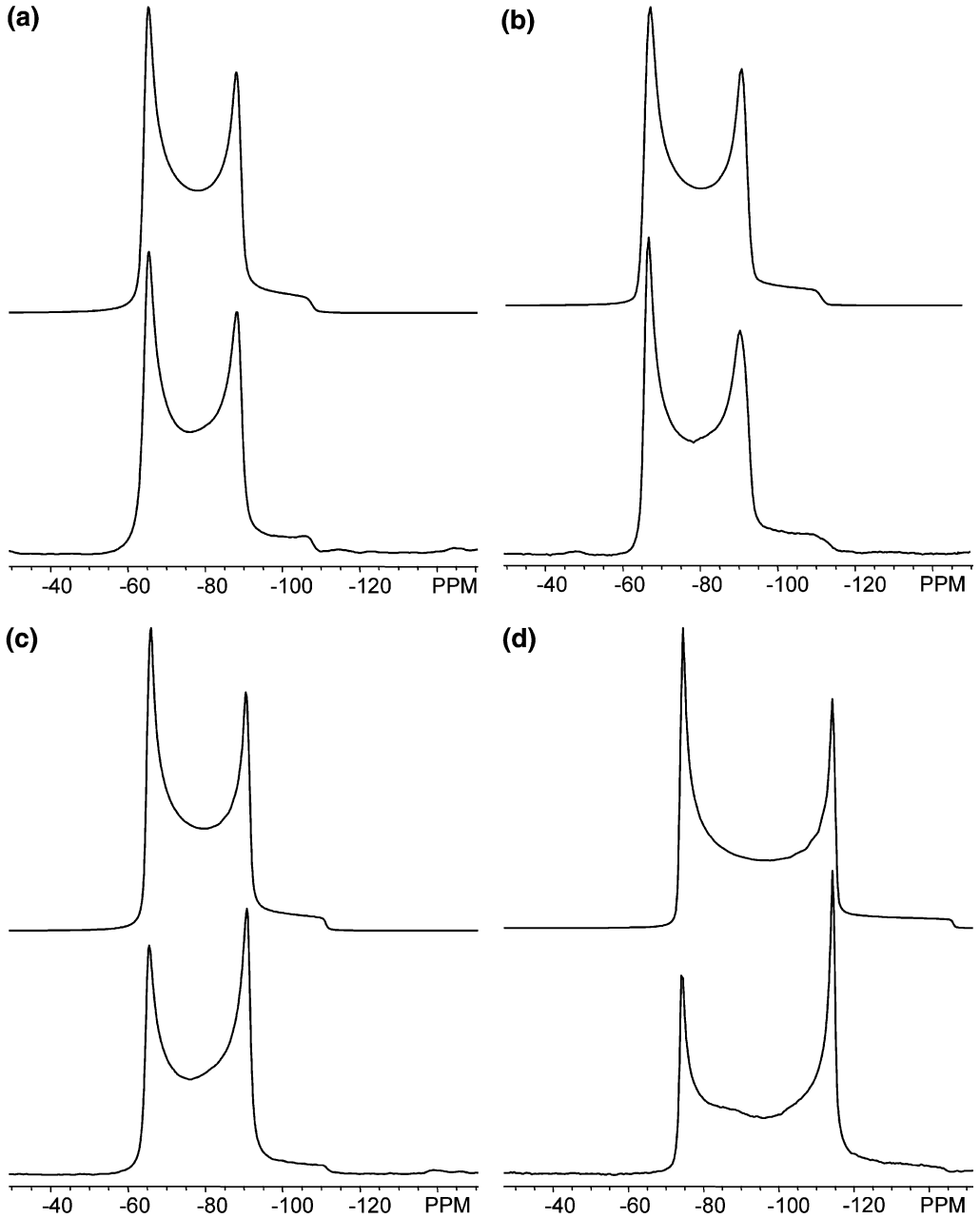

Figure 3. Experimental (bottom trace) and simulated (upper trace) ^{23}Na MAS NMR spectra, acquired at a spinning speed of 14 kHz, of (a) CpNa, (b) Cp^{Me}Na, (c) Cp^{iPr}Na and (d) Cp*Na. See Table 1 for simulation parameters.

the sodium atom in the asymmetric unit. Charges were assigned on the basis of the Mulliken population analysis obtained from single-point energy calculations, with the total sum of all charges on all of the atoms in the lattice equal approximately to zero. Values of C_Q were obtained from the theoretical EFG tensor and converted from atomic units (au) to MHz[40,41] by multiplying V_{33}, the largest component of the EFG tensor, by $(eQ/h)(9.7177 \times 10^{21}$ V m$^{-2})$, where $e = 1.602 \times 10^{-19}$ C and $Q(^{23}\text{Na}) = 1.0 \times 10^{-29}$ m^2.[22]

Chemical shielding tensors were calculated using the GIAO (gauge including atomic orbital) method.[42] In order to reference the calculated sodium chemical shifts with respect to a standard, GIAO calculations were carried out on the hydrated sodium ion, $[Na(H_2O)_6]^+$, which was geometry optimized at all aforementioned levels of theory. The chemical shift of the hydrated sodium ion was set to 0.0 ppm, and from this, the chemical shifts of the Cp′Na compounds were calculated from the relation $\delta_{iso} \approx \sigma_{ref} - \sigma_{sample}$.

Results and Discussion

Solid-State NMR. *Solid-State ^{23}Na MAS NMR.* Experimental and simulated ^{23}Na MAS spectra of all base-free compounds acquired with $\nu_{rot} = 14$ kHz are shown in Figure 3. The values of C_Q, η_Q and δ_{iso} were extracted from the simulation of the MAS NMR spectra. Simulation of the static spectra (discussed below) allows for determination of the anisotropic chemical shielding parameters, Ω and κ. The parameters are summarized in Table 1.

Simulation of the central transition of the ^{23}Na MAS NMR spectrum of CpNa yields $C_Q = 2.97(3)$ MHz, $\eta_Q = 0.02(2)$ and $\delta_{iso} = -57.5(3)$ ppm. The near zero asymmetry parameter reflects the almost linear structure of CpNa ($Cp_{cent}-Na-Cp_{cent}$ angle of 177.7°). Single substitution of the Cp ring by a methyl group causes a slight increase in the quadrupolar interaction as shown in the ^{23}Na MAS NMR spectrum of Cp^{Me}Na. Simulation of the spectrum reveals a larger $C_Q = 3.07(2)$ MHz, $\eta_Q =$

TABLE 1: Experimental ^{23}Na Electric Field Gradient and Chemical Shielding Parameters

compound	C_Q (MHz)	η_Q	δ_{iso} (ppm)	Ω (ppm)[a]	κ[b]
CpNa	2.97(3)	0.02(2)	−57.5(3)	12.5(3.0)	1.0
$Cp^{Me}Na$	3.07(2)	0.05(2)	−58.6(2)	12.5(2.0)	1.0
$Cp^{iPr}Na$	3.14(2)	0.04(3)	−57.0(3)	9.5(2.0)	1.0
Cp*Na	3.89(1)	0.02(2)	−61.9(2)	12.0(3.0)	1.0
CpNa·THF	1.82(2)	0.39(2)	−45.5(2)		

[a] Span of the chemical shift tensor, $\Omega = \delta_{11} - \delta_{33}$. [b] Skew of the chemical shift tensor, $\kappa = 3(\delta_{22} - \delta_{iso})/\Omega$. Due to the relatively small influence of the chemical shielding anisotropy on the appearance of ^{23}Na static patterns, the errors on the skew are large (usually 0.2−0.7, where discernible). From molecular symmetry, κ near 1.0 can be assumed. See text for details.

0.05(2) and $\delta_{iso} = -58.6(2)$ ppm, indicating that the sodium nucleus is slightly more shielded.

Similar parameters were obtained from the ^{23}Na MAS NMR spectrum of $Cp^{iPr}Na$. Due to the increasing magnitude of the quadrupolar interaction, uniform excitation of the powder pattern becomes more difficult. In Figure 3c, the leftmost discontinuity in the $Cp^{iPr}Na$ spectrum is, as a result of the larger C_Q, decreased in intensity with respect to the theoretical powder pattern. Crystallites with different orientations in the powder sample have different orientation-dependent quadrupolar shifts and nutation frequencies (i.e., the frequencies at which the spins precess about the applied rf field).[43] Nutation frequencies range from $2\sin\omega_1 t$ for $C_Q \approx 0$ to $\sin 2\omega_1 t$ for $C_Q \gg \omega_1$. This is further complicated by the fact that, under conditions of MAS, the quadrupolar interaction is partially averaged during the pulse and is time-dependent.[44] In an attempt to rectify this problem, a variety of pulse widths, rf strengths, spinning speeds, as well as rotor-synchronized Hahn-echo experiments, were tested. All attempts failed to increase the intensity of the high-frequency discontinuity to match simulated spectra. Despite the fact that the intensities of the peaks do not match exactly with the theoretical spectrum, the positions of the discontinuities and shoulders in the second-order quadrupolar MAS powder pattern accurately reflect the magnitudes of C_Q, η_Q and δ_{iso}.

Simulation of the ^{23}Na MAS NMR spectrum of Cp*Na reveals a much larger C_Q compared to other $[Cp'Na]_n$ complexes, with $C_Q = 3.89(1)$ MHz. The EFG tensor has near axial symmetry, as in all of the other compounds, with $\eta_Q = 0.02(2)$. The sodium nucleus is slightly more shielded compared to that in CpNa at −61.9(2) ppm. Due to the larger C_Q, there was difficulty in using single-pulse experiments to obtain MAS powder patterns without dramatic base-line distortions, because of loss of points at the beginning of the FID. As a result, rotor-synchronized Hahn-echo experiments were used for Cp*Na, which provided excellent line shapes with minimal base-line distortion (Figure 3d); however, the high-frequency discontinuity is lower in intensity than that observed in simulations, for reasons discussed above.

Relationships between NMR Parameters and Molecular Structure. It is obvious from the experimental NMR data presented herein that increasing substitution of the Cp ring in the linear sodocenes results in an increase in the ^{23}Na quadrupolar interaction. The main structural difference between the known crystal structures of CpNa and Cp*Na is the Cp'_{cent}−Na distance. In CpNa, this distance is 2.357 Å, whereas the rings are closer to the sodium center in Cp*Na, with a Cp'_{cent}−Na distance of 2.3057 Å. Is it the substitution of the Cp′ rings, the proximity of the rings to the sodium atom, the local symmetry about the central sodium atom or a combination of these factors which causes the increase in the quadrupolar interaction as substitution of the ring increases?

It has been shown that the magnitude of the largest component of the EFG tensor at a nucleus within a molecule or ionic solid is related to the spherical symmetry about that nucleus.[45] For example, specific combinations of tetrahedral, octahedral, dodecahedral, or icosahedral sites will produce a negligible EFG at a centrosymmetric position.[46] All of the linear $[Cp'Na]_n$ molecules studied within this work are not spherically symmetric about the Na atoms and, as a result, will have large V_{33} components and correspondingly large values of C_Q. In a previously published communication, a value of $C_Q(^{23}Na) = 1.8$ MHz was reported for the base-substituted *N,N,N′,N′*-tetramethylethylenediamine sodiumcyclopentadienide (CpNa-TMEDA),[19] which has a Cp_{cent}−Na−Cp_{cent} angle on the order of 128.1°.[47] The authors of this paper do not report δ_{iso} or η_Q, though the appearance of the powder pattern suggests an EFG tensor of relatively high axial symmetry. The bent structure and less spherically symmetric environment of the ^{23}Na nucleus in the CpNa-TMEDA molecule might suggest a larger value of C_Q in this compound in comparison to the linear, axially symmetric CpNa and Cp*Na molecules. However, we believe that the low C_Q for the TMEDA complex results predominantly from the large Cp_{cent}−Na distance of 2.667 Å. Thus, the value of C_Q decreases in the order Cp*Na > CpNa > CpNa-TMEDA as the Cp_{cent}−Na distance increases. Axially symmetric EFG tensors are measured for CpNa and Cp*Na, due to the near-linear ...−Cp−Na−Cp−Na−... arrangement and the pseudo-cylindrical symmetry about the Na sites. The structures of singly substituted $Cp^{Me}Na$ and $Cp^{iPr}Na$ compounds have not been determined; however, the ^{23}Na quadrupolar parameters strongly suggest that these complexes have linear chains of η^5-Cp rings and Na sites and that the Cp'_{cent}−Na distances are smaller than those in CpNa but larger than those in Cp*Na. The relationship between the C_Q and the Cp'_{cent}−Na distance is further probed in the theoretical portion of the Results and Discussion.

The sodium nuclei in the linear compounds are extremely shielded with respect to the usual ^{23}Na chemical shift range, with values of δ_{iso} ranging from −57.3 to −61.9 ppm. The bulky Cp* ligand serves to slightly increase the shielding at the ^{23}Na nucleus in comparison to the less-substituted Cp′ ligands. The high magnetic shielding at the metal nucleus generally encountered in NMR spectra of metallocenes cannot be simply attributed to the high electron density of the π-electron systems of the Cp′ rings; rather, theoretical studies on ferrocene[48] and the aluminocenium cation[20] reveal that magnetic shielding of the central metal nucleus results from a variety of factors, notably the magnetic-dipole-allowed mixing of occupied and virtual molecular orbitals. A full molecular orbital analysis of the origin of chemical shielding in polymeric sodocenes is beyond the scope of this paper, though some preliminary calculations are presented in the theoretical portion of the Results and Discussion within this paper.

Solid-State ^{23}Na Static NMR Experiments. The static ^{23}Na spectra for all compounds are shown in Figure 4. All spectra were simulated to include the effects of anisotropic chemical shielding, setting the Euler angles $\alpha = \beta = \gamma = 0°$ (implying that the most shielded component of the CS tensor δ_{33} and the largest component of the EFG tensor V_{33} are collinear) and $\kappa = 1$ (meaning that $\delta_{11} = \delta_{22}$ and that δ_{33} is the unique principal component of the CS tensor). All compounds show some degree of sodium CSA, which ranges from $\Omega = 9.5(2.0)$ ppm for $Cp^{iPr}Na$ to slightly larger spans of $\Omega = 12-12.5$ ppm for other compounds.

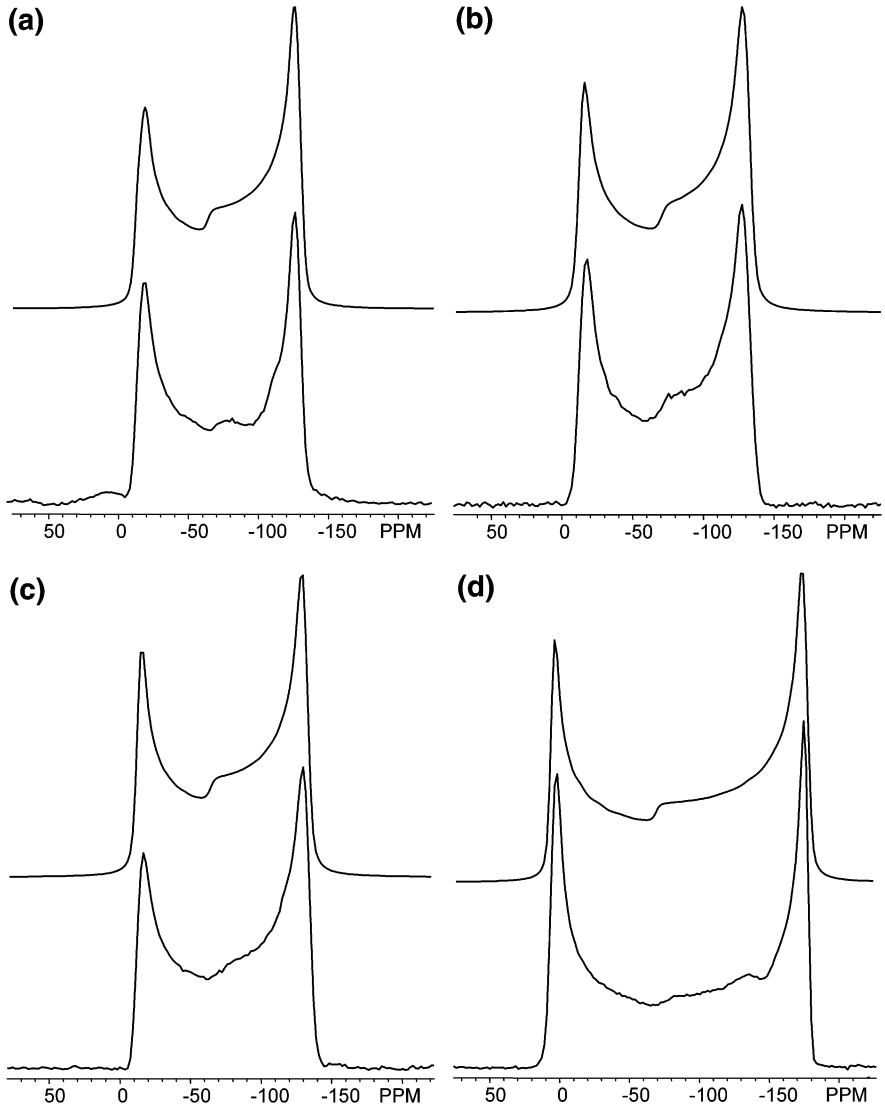

Figure 4. Experimental (bottom trace) and simulated (upper trace) ^{23}Na static NMR spectra of (a) CpNa, (b) Cp^{Me}Na, (c) Cp^{iPr}Na and (d) Cp*Na. See Table 1 for simulation parameters.

There are very few examples of sodium CSA reported in the literature, due to the fact that Na^+ has relatively nonpolarizable valence orbitals and is rarely involved in covalent bonding of any kind. To the best of our knowledge, only four examples have been reported in the literature, the largest being 19 ppm.[49−51] Large ^{23}Na second-order quadrupolar effects often dominate the static powder patterns, and the sodium CSA contributions are relatively small by comparison. For example, the breadth of the base of the static powder pattern of Cp^{Me}Na is 14.1 kHz wide, where only 0.7 kHz is contributed by the CSA, accounting for ca. 5% of the breadth of the static pattern. As a result, it is difficult to accurately calculate κ, and the errors in the calculated values of Ω are large. Increasingly accurate measurement of the anisotropic sodium chemical shielding parameters in these molecules would require acquisition of additional spectra at a higher magnetic field (e.g., 18.8 T), where the contributions of the quadrupolar and chemical shielding interactions to the breadth of the ^{23}Na NMR powder patterns are scaled by $1/B_0$ and B_0, respectively. Nonetheless, it is evident that there is some effect from sodium CSA present in the ^{23}Na NMR spectra of these molecules.

To obtain a static spectrum that accurately reflects the contributions from both anisotropic chemical shielding and quadrupolar interactions, great care must be taken in ensuring that the proper experimental conditions are chosen to uniformly excite the broad ^{23}Na powder patterns. We have found that, for moderately wide powder patterns (15−20 kHz), using a large rf field in a Hahn-echo static experiment results in a poor line shape (Figure 5). It is evident that using large rf fields (e.g., $\nu_1 = 86$ kHz) results in a dramatic dip in the powder pattern just before the rightmost (low frequency) discontinuity. This effect is due to nutation distortions in regions of the spectrum where the fictitious spin-1/2 hypothesis (i.e., for pulse width τ_p, central transition selective pulses have a tip angle $\theta_s = \theta_{ns}(I + {}^1/_2)^{-1}\nu_1\tau_p$, when $\nu_1 \ll \nu_Q$ and θ_{ns} is the tip angle for nonselective excitation)[52] is not valid, since for some crystallite orientations, $\nu_1 > \nu_Q$. The best line shape was achieved using a very small rf field of only 7 kHz, in accordance with the observations of Amoureux and co-workers.[53] Since a smaller B_1 field is being applied, some signal-to-noise is lost in the process, and the acquisition of a greater number of transients is required. Uniform excitation with small rf fields is essential when the exact shape of the NMR powder pattern must be acquired for deconvolution of contributions from the quadrupolar and chemical shielding interactions,[53,54] as evidenced in Figures 4 and 5.

Variable-Temperature Solid-State ^{23}Na NMR. The variable-temperature ^{23}Na spectra of Cp^{iPr}Na (Figure 6) are typical of

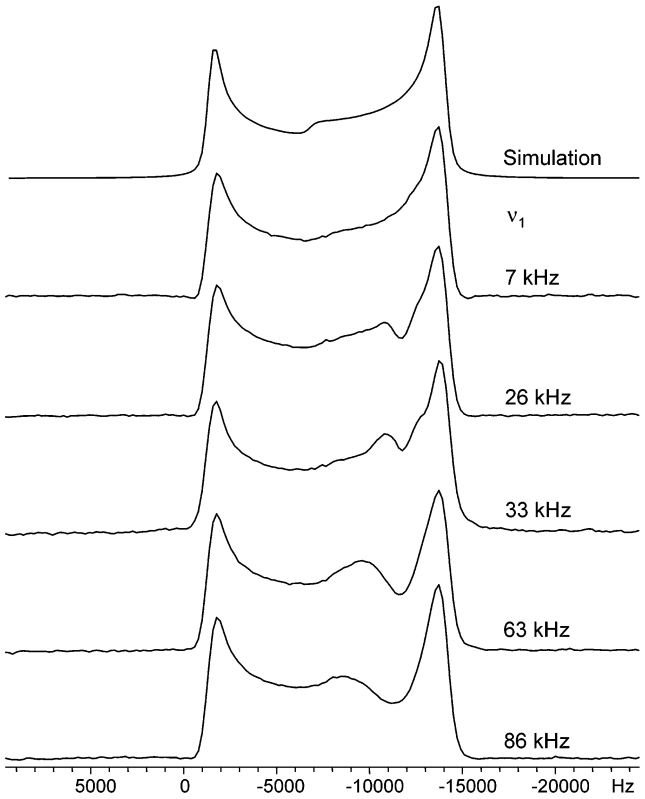

Figure 5. ^{23}Na static NMR spectra of Cp$^{i\mathrm{Pr}}$Na, obtained using variable rf strengths.

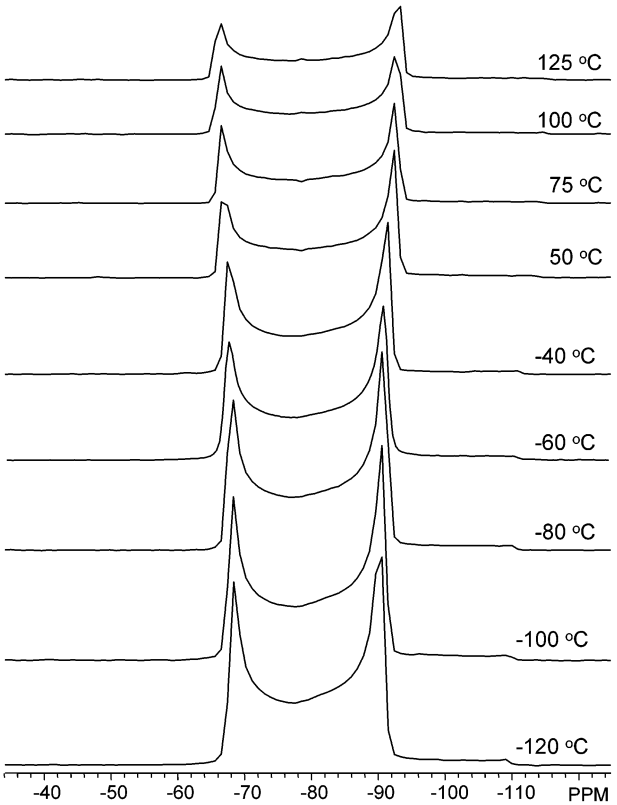

Figure 6. Variable-temperature ^{23}Na MAS NMR spectra of Cp$^{i\mathrm{Pr}}$Na, acquired with a spinning speed of 8.2 kHz.

the appearance of the spectra for all compounds. All spectra were acquired with the same number of scans and become noticeably more intense as the temperature is decreased, due to the Boltzmann distribution. The chemical shifts of all compounds are temperature dependent (Figure 7a). As the temperature is increased there is a positive increase in the chemical shift for all compounds (i.e., the sodium nucleus becomes slightly deshielded). There appears to be a relationship between chemical shift, temperature and the substitution of the Cp′ rings: as the substitution and steric bulk of the Cp′ ring increases, the dependence of the chemical shift on temperature decreases. This is shown by the fact that the greatest temperature dependence is found for CpNa, with a slope of 1.56 ppm/100 °C, then Cp$^{\mathrm{Me}}$Na at 1.54 ppm/100 °C, Cp$^{i\mathrm{Pr}}$Na at 1.51 ppm/100 °C and Cp*Na at 0.891 ppm/100 °C. This change in δ_{iso} with temperature is separate from the quadrupolar induced shifts of the powder pattern, because the calculated spectra for each temperature take into account contributions from the chemical shielding and quadrupolar interaction simultaneously. Interestingly, all compounds displayed a linear increase in C_Q with increasing temperature, as shown in Figure 7b. This temperature dependence appears to have no observable relation to the nature of the substitution of the Cp ring. The smallest rate of C_Q increase was found for singly substituted Cp$^{\mathrm{Me}}$Na at 0.080 MHz per 100 °C, whereas the largest rate was determined to be 0.120 MHz per 100 °C for Cp$^{i\mathrm{Pr}}$Na.

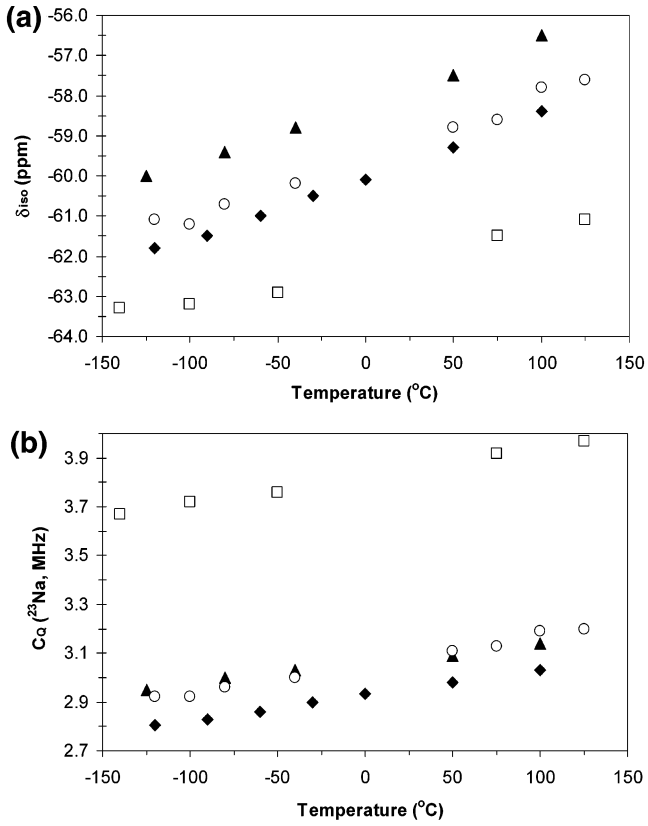

Figure 7. Plot of the variation of (a) δ_{iso} (^{23}Na) and (b) C_Q (^{23}Na) of (◆) CpNa, (▲) Cp$^{\mathrm{Me}}$Na, (○) Cp$^{i\mathrm{Pr}}$Na and (□) Cp*Na with temperature.

In the many previous variable-temperature NMR studies on half-integer quadrupolar nuclei, C_Q is normally observed to increase with decreasing temperature. This is commonly attributed to slowing down of vibrations and rotations in molecules or ionic solids which serve to rapidly change the directions of the axes of the EFG tensor at higher temperatures, often resulting in a reduction in the magnitude of C_Q.[55,56] Variable-temperature ^{23}Na NMR experiments on a variety of systems, including sodium orthophosphate,[57] crown ether alkalides,[58] sodalites,[59] and sodium-containing minerals,[60] all show that C_Q(^{23}Na) decreases with increasing temperature. However, there are some instances reported for other half-integer quadrupolar nuclei in

TABLE 2: Experimental Carbon Chemical Shift Tensors

compound	carbon	δ_{11} (ppm)	δ_{22} (ppm)	δ_{33} (ppm)	δ_{iso} (ppm)	Ω (ppm)[a]	κ[b]
CpNa	Cp	141.0	138.8	33.8	104.5	107.1	0.96
$Cp^{Me}Na$	Cp *i*	161.7	146.4	37.4	115.2	124.3	0.75
	Cp *o*/*m*	139.3	129.6	42.2	103.7	97.1	0.80
	Me				14.5		
$Cp^{iPr}Na$	Cp *i*	174.6	173.7	40.4	129.6	134.2	0.98
	Cp *o*	157.3	113.6	38.3	103.1	119.1	0.27
	Cp *m*	162.0	104.1	37.4	101.2	124.5	0.07
	*i*Pr Me				29.9		
	*i*Pr Me				27.5		
Cp*Na	Cp	139.8	137.9	35.9	104.6	103.9	0.96
	Me				9.5		
CpNa·THF[c]	Cp				104.5		

[a] Span of the chemical shift tensor, $\Omega = \delta_{11} - \delta_{33}$. [b] Skew of the chemical shift tensor, $\kappa = 3(\delta_{22} - \delta_{iso})/\Omega$. [c] Analysis of carbon chemical shift tensor not available, since the complex is in a mixture with CpNa.

which increasing values of C_Q are observed with increasing temperature.[61] It might be anticipated that an increased rate of rotation of the Cp′ rings in the $[Cp'Na]_n$ compounds with increasing temperature would result in a reduction of the V_{33} component of the EFG tensor and therefore in a reduced value of C_Q. At room temperature, rotation of the Cp rings about the central metal atom in metallocenes is fast with respect to the NMR time scale (as shown in ^{13}C NMR spectra in this paper and in previous studies on metallocenes).[62−64] However, due to the generally low rotational barriers in such compounds (2−12 kJ mol^{-1}),[12] the electronic character of the Cp′ rings should not change significantly with rotation. In addition, V_{33} is directed along the C_5-symmetry axis of the metallocene, and Cp′ rotation should have very little effect on C_Q.

From room-temperature ^{23}Na MAS NMR experiments, it is observed that C_Q increases with increasing substitution of the Cp ring. Furthermore, we know that the Cp'_{cent}−Na distance is smaller in Cp*Na than that in CpNa and that the C_Q is much larger for the former complex. Similarly, CpNa has a much smaller Cp_{cent}−Na distance and a much larger C_Q than that for CpNa-TMEDA. Thus, we believe that, with increasing temperature, the Cp'_{cent}−Na distance decreases in all of the linear $[Cp'Na]_n$ complexes, resulting in a corresponding increase in C_Q. The precise reason for the decrease of this distance at higher temperatures is unknown. It is possible that, if Cp'_{cent}−Na distances decrease with increasing temperature, there may be some correlated uniaxial compression of the unit cell along the direction of the Cp′Na chains. The relationship between the Cp'_{cent}−Na distance, the nature of the Cp′ ligand, and C_Q is further explored using ab initio calculations (vide infra).

Solid-State ^{13}C CPMAS NMR. Chemical shift parameters for all compounds are summarized in Table 2. The ^{13}C CPMAS NMR spectra of CpNa and Cp*Na are shown in parts a and b of Figure 8, respectively. Both spectra have one isotropic peak and corresponding manifold of spinning sidebands corresponding to Cp′ ring carbons, since all of these carbon sites are equivalent due to rapid rotation of the Cp′ rings. Isotropic resonances for the aromatic carbon sites are observed at $\delta_{iso}(^{13}C) = 104.5$ ppm for CpNa and $\delta_{iso}(^{13}C) = 104.6$ ppm for Cp*Na. A single isotropic resonance is also observed for the methyl carbons of the Cp* ring in Cp*Na, with $\delta_{iso}(^{13}C) = 9.5$ ppm. The ^{13}C CPMAS NMR spectra of $Cp^{Me}Na$ and $Cp^{iPr}Na$ are slightly more complicated than those of the aforementioned compounds (parts c and d of Figure 8, respectively). Single substitution of the Cp ring results in three inequivalent sites, denoted as ipso, ortho, and meta. All three sites are clearly visible in the $Cp^{iPr}Na$ spectrum, but the ortho and meta sites could not be separately resolved for $Cp^{Me}Na$. The inability to resolve these sites is likely due to their similarity and apparent lack of a microcrystalline structure.

The ^{13}C chemical shielding tensors were determined for these compounds by Herzfeld−Berger analysis[65] of slow-spinning ^{13}C CPMAS spectra. In all cases, the measured spans of the carbon chemical shielding tensors, Ω, are similar to one another and to carbon CS tensors in a variety of axially symmetric metallocenes.[62,66,67] Both CpNa and Cp*Na have almost axially symmetric carbon chemical shielding tensors, with $\kappa = 0.96$, corresponding to the rapid rotation of the Cp′ rings. For $Cp^{iPr}Na$ and $Cp^{Me}Na$, the values of κ show some deviation of the CS tensor away from axial symmetry, likely due to the asymmetric substitution of the Cp rings therein.

Variable-Temperature Solid-State ^{13}C CPMAS NMR. Variable-temperature ^{13}C CPMAS experiments were performed on CpNa and Cp*Na. Analysis of the spinning sideband manifolds in all cases reveals that Ω remains relatively constant at all temperatures and that κ is always close to 1.0. These results are not surprising, given that the low rotational barriers of the Cp′ rings would require extremely low temperatures to slow ring rotation to the point where a powder pattern dominated by a modest carbon CSA would exhibit such dynamic effects.[62] On the basis of the symmetry of the Cp′ rings, the CS tensors of the aromatic ring carbons should have three unique components: one perpendicular to the plane of the ring, one directed along the C−H or $C-CH_3$ bond, and the final component oriented perpendicular to the bond in the plane of the ring. In theory, the symmetry of the molecule should result in a nonaxially symmetric ^{13}C powder pattern largely dominated by the anisotropic chemical shielding interaction. However, the rapid ring rotation averages the effects of the carbon shielding tensor on the ^{13}C powder pattern, meaning that the similarity in δ_{11} and δ_{22} results from an averaging of these two tensor components due to rapid rotation of the Cp′ rings. Since δ_{33} is perpendicular to the plane of the rings, it is unaffected by this rotation; hence, the ^{13}C powder pattern appears as an axially symmetric carbon shielding tensor. These results are discussed further in the ab initio section of the Results and Discussion.

Solid-State ^{23}Na MAS, ^{13}C CPMAS, and Variable-Temperature ^{23}Na MAS NMR of a Mixture of CpNa and CpNa·THF. It has been hypothesized that THF has the ability to bind directly to the central sodium atom in CpNa and Cp*Na.[2] However, due to the inability of these molecules to form crystals that are suitable for diffraction studies, there is no definitive proof of this in the solid state. However, there are reported crystal structures for a variety of polymeric substituted cyclopentadienylsodium metallocenes,[68−71] as well as for an anionic C−C bridged *ansa*-sodocene sandwich complex, $[Me_4C_2Cp_2Na^-\cdot THF][PPh_4^+]$, which are solvated with a single THF ligand at the sodium atom.[72] A combination of ^{23}Na and ^{13}C solid-state NMR experiments conducted upon a rapidly recrystallized sample of CpNa from THF shows that the THF ligand coordinates to some of the sodium atoms. On the basis of quadrupolar parameters, sodium chemical shifts, ^{13}C NMR data, and variable-temperature ^{23}Na NMR experiments, we are able to propose a structure for CpNa·THF (Figure 1c), which is similar to both the CpNa·TMEDA and $[Me_4C_2Cp_2Na^-\cdot THF][PPh_4^+]$ complexes.[72,73] In this structure, the [CpNa] units zigzag back and forth, while a THF molecule coordinates to each sodium atom. Discussion of the relationship between the NMR parameters and this proposed structure follows.

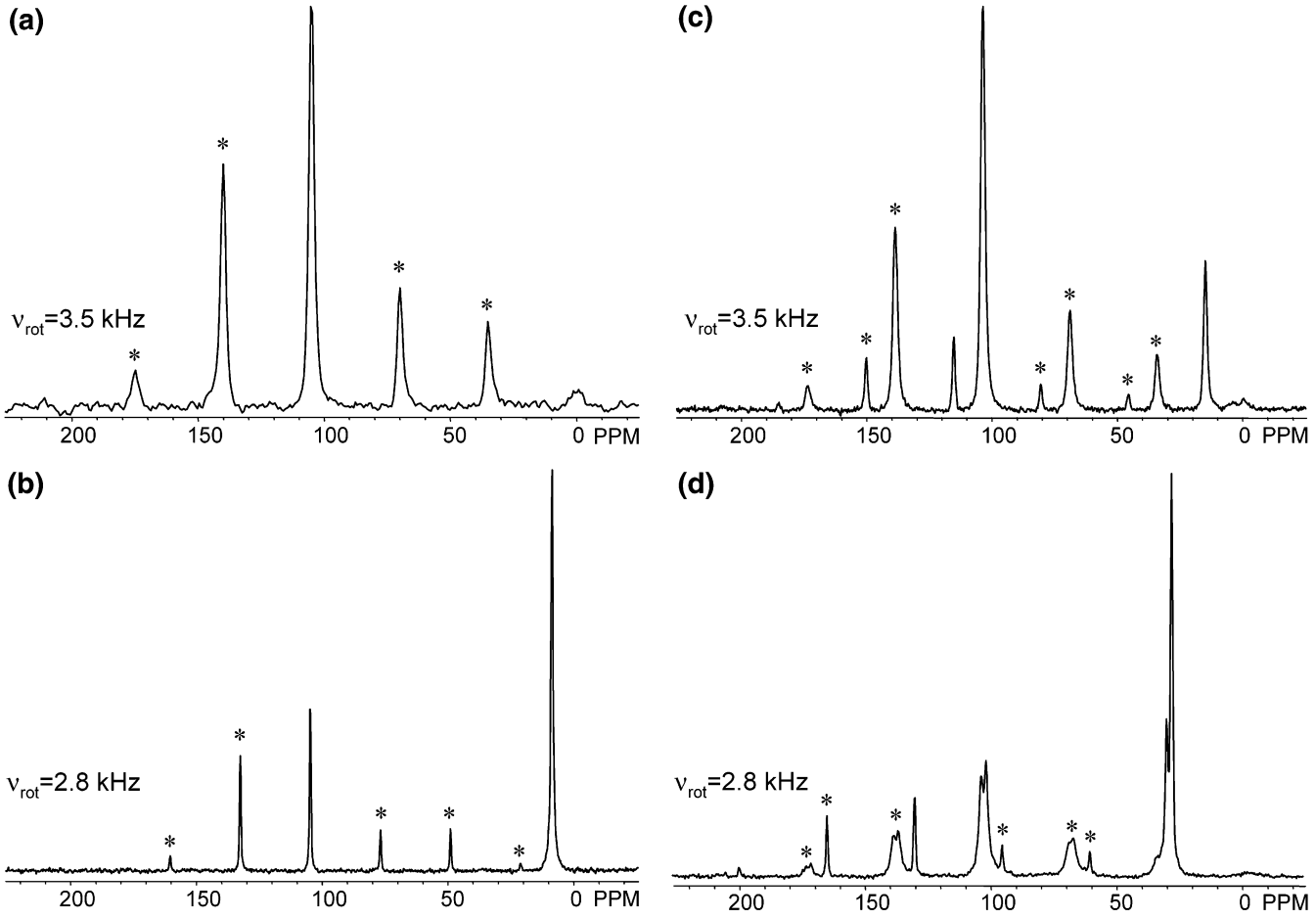

Figure 8. ^{13}C CPMAS NMR spectra of (a) CpNa, (b) Cp*Na, (c) Cp^{Me}Na and (d) Cp^{iPr}Na.

The ^{23}Na MAS NMR spectrum of rapidly recrystallized CpNa (Figure 9b) reveals a mixture of CpNa and the proposed CpNa·THF species. The powder pattern of the latter compound differs substantially from that of CpNa, as confirmed by simulations of the central transition MAS powder pattern which yield $\delta_{iso} = -45.5(2)$ ppm, $C_Q = 1.82(2)$ MHz and $\eta_Q = 0.39(2)$. The isotropic shift still indicates a very shielded sodium nucleus, implying that this pattern corresponds to a sodium metallocene species. The reduced C_Q and nonaxially symmetric η_Q imply the presence of a sodium atom in a distinct electronic environment. To confirm the presence of the CpNa·THF species, ^{13}C CPMAS NMR experiments were conducted. A single resonance observed at $\delta_{iso}(^{13}C) = 104.5$ ppm is the same as that measured for pure CpNa (Figure 9a). Thus, the two species must possess similarly coordinated η^5-Cp rings. There are two additional resonances at 66.1 and 24.7 ppm, which correspond, within experimental error, to the accepted values for THF.[74] The ^{23}Na and ^{13}C NMR spectra therefore indicate the presence of two species with a similar ligand chemistry, but with very distinct structures, about the central sodium atom.

The decrease in the value of $C_Q(^{23}Na)$ in CpNa·THF with respect to CpNa is likely due to the longer $Cp_{cent}-Na$ distance in the former. Our hypothesized structure for this species is supported by the fact that the larger $Cp_{cent}-Na$ distance of 2.691 Å in CpNa·TMEDA,[73] compared to that of 2.357 Å for CpNa, results in a $C_Q = 1.8$ MHz,[19] a value very similar to that of CpNa·THF. The increase in the $Cp_{cent}-Na$ distance is thought to arise from the Cp rings moving away from the sodium in an attempt to minimize steric interactions with one another as well as with the coordinated THF ligand. The nonzero asymmetry parameter implies that the electronic environment about the sodium atom is no longer axially symmetric. Unfortunately, no asymmetry parameter was reported for CpNa·TMEDA for comparison.[19]

An interesting phenomenon is observed in the variable-temperature ^{23}Na MAS experiments performed on the mixture of CpNa and CpNa·THF (Figures 10 and 11). Unlike CpNa, where the C_Q increases considerably with increasing temperature, the C_Q for CpNa·THF stays relatively constant upon heating. However, η_Q decreases dramatically as the temperature is increased. The constant value of C_Q with changing temperature suggests that the distance between the sodium atom and the Cp rings stays relatively constant. The change in the asymmetry parameter likely results from bending about the sodium atom (i.e., a decrease in the $Cp_{cent}-Na-Cp_{cent}$ angle) as the temperature is altered. Assuming a crystallographic axis runs parallel to the direction of the linear or zigzagging [Cp′Na] units, it seems that this axis must undergo temperature dependent shortening and lengthening that is significantly different from the perpendicular unit cell axes. Variable-temperature data on both linear and bent species would therefore seem to suggest an uniaxial compression of the $[Cp'Na]_n$ chains with increasing temperature, regardless of whether they have a linear or zigzagging structure.

Ab Initio Calculations. *Ab Initio Study of ^{23}Na EFG Tensors in Linear Sodocenes.* Ab initio calculations on extremely long Cp−Na chains were not conducted due to the fact that computation times quickly become prohibitive as the size of the chain is increased. Calculations were performed upon a variety of small clusters, as well as upon clusters embedded

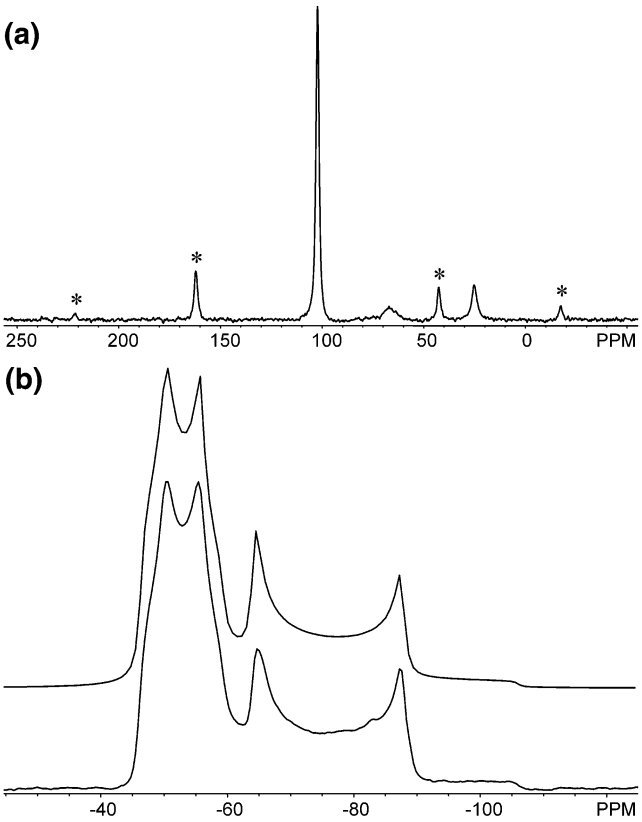

Figure 9. (a) ^{13}C CPMAS NMR spectrum (ν_{rot} = 3.5 kHz) and (b) experimental (lower trace) and simulated (upper trace) ^{23}Na MAS NMR spectra of a mixture of CpNa·THF and CpNa (ν_{rot} = 9.0 kHz). See Table 1 for ^{23}Na simulation parameters.

within lattices of point charges (embedded cluster molecular orbital calculations, ECMO[39]), to see which models best predict the values of C_Q and η_Q while simultaneously reducing computational time. Calculations were performed only on CpNa and Cp*Na clusters, since solid-state structures were available for these compounds. NMR calculations on structures from full geometry optimizations of CpNa and Cp*Na are not reported nor deemed important, as the solid-state and gas phase structures differ considerably. Full geometry optimizations result in the Cp′ rings moving away from the sodium ions (when it is possible to obtain convergence of the calculation), thereby drastically influencing the structure and nature of the calculated NMR interaction tensors. Cluster sizes varied from Cp_2Na^- to $Cp_4Na_5^+$ for CpNa and from $Cp^*_2Na^-$ to $Cp^*_2Na_3^+$ for Cp*Na. For example, the Cp_2Na^- cluster is the linear chain Cp−Na−Cp, where Cp is the terminal unit, and $Cp_2Na_3^+$ is the Na−Cp−Na−Cp−Na chain, where sodium is the terminal unit. Calculations were not conducted on single Cp−Na or Cp*−Na clusters nor upon "lopsided" structures (e.g., Cp−Na−Cp− Na), as they do not accurately reflect the electronic environment at the sodium atom and are associated with difficulties in obtaining converging SCF calculations. ECMO calculations on CpNa, in which the isolated molecular cluster is embedded within a lattice of point charges, yield EFG tensors almost identical to those from calculations on isolated clusters, implying that long-range effects on the EFG tensor from neighboring $[CpNa]_n$ chains are negligible. ECMO calculations were not conducted upon Cp*Na clusters since Cp*Na has larger interchain distances than CpNa. Results from some of the calculations conducted on these clusters are presented in Tables 3 and 4.

The Asymmetry Parameter (η_Q). Theoretical calculations performed on isolated CpNa and Cp*Na clusters, as well as ECMO calculations, predict near-zero values (i.e., almost perfect axial symmetry) at all levels of theory, in good agreement with experimental values. Variation of the cluster size has very little effect on the calculated asymmetry parameters.

The Quadrupolar Coupling Constant (C_Q). In general, the theoretical quadrupolar coupling constant varies considerably depending on the cluster size, the calculation method, and the basis set. For the smaller 6-31G** basis set, the C_Q increases as the size of the cluster increases up to $Cp_4Na_3^-$. Using the RHF method, the C_Q increases from 2.55 MHz (Cp_2Na^-) to 2.66 MHz ($Cp_2Na_3^+$) to 2.76 MHz ($Cp_4Na_3^-$) and then decreases to 2.72 MHz ($Cp_4Na_5^+$). The choice of cationic or anionic cluster may affect the outcome of the calculation. For instance, calculated values using the larger 6-311G** basis set depend predominantly upon whether the cluster is terminated by the Cp ligand or a sodium atom, as well as upon the size of the cluster. When the cluster is terminated by Cp rings, the resulting C_Q is considerably higher than that when sodium terminates the cluster, and if the cluster is terminated with Cp, the C_Q decreases as the size of the cluster increases. The opposite effect occurs when sodium atoms are terminal. The ECMO calculations followed the above trends, and the results varied insignificantly from the isolated cluster calculations.

Cp*Na exists as both an eclipsed and a partially eclipsed (13.89°) molecule in its polcrystalline form. Due to the increased size of the Cp* ligand with respect to Cp, calculations on species larger than $Cp^*_2Na_3^+$ were not feasible. Thus, calculations were performed only on isolated $Cp^*_2Na^-$ and $Cp^*_2Na_3^+$ clusters. The best agreement between theory and experiment is found in both RHF and B3LYP calculations using the 6-311G** basis set. The values of C_Q are almost identical for the eclipsed and partially eclipsed geometries. Results from the calculations on Cp*Na follow the same trends found for those on CpNa: with the 6-311G** basis set, when Cp* is terminal, the calculated values of C_Q are larger than that if sodium is terminal. With the 6-31G** basis set, C_Q increases with increasing cluster size. In all cases, the RHF calculations predict larger values of C_Q than those predicted by B3LYP calculations.

In summary, RHF/6-311G** calculations on isolated Cp_2Na^- and $Cp^*_2Na_3^+$ clusters yield C_Q values which are closest to the experimentally determined values. EFG tensor calculations are clearly quite difficult for molecules such as CpNa and Cp*Na, since one must attempt to take into account long-range intermolecular interactions, as well as to determine a proper method for chain termination that will not unnecessarily lengthen computational time or render the molecular environment as being unrealistic. The cationic or anionic charge on the cluster may have some influence on the calculated EFG tensor parameters as well. Nonetheless, the calculations qualitatively predict an increase in the quadrupolar interaction in the Cp*Na clusters compared to CpNa clusters at all levels of theory, in agreement with experimental results.

Sodium Chemical Shielding. Calculations of chemical shielding tensors were performed on CpNa and Cp*Na using various cluster sizes, methods and basis sets, as described above (Tables 5 and 6). The calculated span and skew are relatively consistent for all CpNa calculations and close to the experimentally determined values. Notably, the RHF calculations seem the most consistent in predicting Ω. As cluster size is increased, the magnitude of the span decreases at all levels of theory. Very good agreement is found between experimental and theoretical RHF/6-311G** isotropic sodium chemical shifts, whereas

TABLE 3: Theoretical ^{23}Na Electric Field Gradient Tensors in CpNa

molecule	lattice[a]	method	basis set	C_Q (MHz)[b]	η_Q	V_{11} (au)	V_{22} (au)	V_{33} (au)
CpNa		exptl		2.97(3)	0.02(2)			
Cp_2Na^-	no	B3LYP	6-31G**	1.4568	0.0050	−0.0308	−0.0312	0.0620
Cp_2Na^-	yes	B3LYP	6-31G**	1.4339	0.0147	−0.0301	−0.0310	0.0610
$Cp_2Na_3^+$	no	B3LYP	6-31G**	1.4433	0.0053	−0.0305	−0.0309	0.0614
$Cp_2Na_3^+$	yes	B3LYP	6-31G**	1.4393	0.0032	−0.0305	−0.0307	0.0613
$Cp_4Na_3^-$	no	B3LYP	6-31G**	1.5459	0.0052	−0.0327	−0.0331	0.0658
$Cp_4Na_5^+$	no	B3LYP	6-31G**	1.4723	0.0043	−0.0312	−0.0315	0.0627
Cp_2Na^-	no	B3LYP	6-311G**	2.6407	0.0038	−0.0560	−0.0564	0.1124
Cp_2Na^-	yes	B3LYP	6-311G**	2.3634	0.0487	−0.0478	−0.0527	0.1006
$Cp_2Na_3^+$	no	B3LYP	6-311G**	2.2845	0.0041	−0.0484	−0.0488	0.0972
$Cp_2Na_3^+$	yes	B3LYP	6-311G**	2.3825	0.0214	−0.0496	−0.0518	0.1014
$Cp_4Na_3^-$	no	B3LYP	6-311G**	2.5029	0.0040	−0.0530	−0.0535	0.1065
$Cp_4Na_5^+$	no	B3LYP	6-311G**	2.4085	0.0033	−0.0511	−0.0514	0.1025
Cp_2Na^-	no	RHF	6-31G**	2.5492	0.0034	−0.0541	−0.0544	0.1085
Cp_2Na^-	yes	RHF	6-31G**	2.4494	0.0016	−0.0520	−0.0522	0.1042
$Cp_2Na_3^+$	no	RHF	6-31G**	2.6595	0.0027	−0.0564	−0.0567	0.1132
$Cp_2Na_3^+$	yes	RHF	6-31G**	2.6864	0.0044	−0.0563	−0.0568	0.1131
$Cp_4Na_3^-$	no	RHF	6-31G**	2.7626	0.0027	−0.0586	−0.0589	0.1176
$Cp_4Na_5^+$	no	RHF	6-31G**	2.7203	0.0027	−0.0577	−0.0580	0.1158
Cp_2Na^-	no	RHF	6-311G**	2.8062	0.0039	−0.0595	−0.0599	0.1194
Cp_2Na^-	yes	RHF	6-311G**	2.5177	0.0467	−0.0511	−0.0561	0.1071
$Cp_2Na_3^+$	no	RHF	6-311G**	2.4419	0.0037	−0.0518	−0.0522	0.1039
$Cp_2Na_3^+$	yes	RHF	6-311G**	2.5388	0.0091	−0.0535	−0.0545	0.1080
$Cp_4Na_3^-$	no	RHF	6-311G**	2.6636	0.0036	−0.0565	−0.0569	0.1134
$Cp_4Na_5^+$	no	RHF	6-311G**	2.6326	0.0035	−0.0558	−0.0562	0.1120

[a] Embedded cluster calculation using a 20 Å sphere of enclosure. [b] Calculated EFG tensors were converted from atomic units (au) to MHz by multiplying the largest component of the EFG tensor V_{33} by $(eQ/h)(9.7177 \times 10^{21}\ \mathrm{V\ m^{-2}})$, where $Q(^{23}\mathrm{Na}) = 1.0 \times 10^{-29}\ \mathrm{m^2}$ and $e = 1.602 \times 10^{-19}$ C.

TABLE 4: Theoretical ^{23}Na Electric Field Gradient Tensors of Cp*Na Clusters

molecule	method	basis set	C_Q (MHz)[a]	η_Q	V_{11} (au)	V_{22} (au)	V_{33} (au)	geometry[b]
Cp*Na	exptl		3.89(1)	0.02(2)				
$Cp^*_2Na^-$	B3LYP	6-31G**	2.4574	0.1046	−0.0521	−0.0525	0.1046	A
$Cp^*_2Na^-$	B3LYP	6-31G**	2.4556	0.0065	−0.0519	−0.0526	0.1045	B
$Cp^*_2Na_3^+$	B3LYP	6-31G**	2.5512	0.0043	−0.0541	−0.0545	0.1086	A
$Cp^*_2Na_3^+$	B3LYP	6-31G**	2.5512	0.0050	−0.0540	−0.0546	0.1086	B
$Cp^*_2Na^-$	B3LYP	6-311G**	4.0907	0.0048	−0.0866	−0.0875	0.1741	A
$Cp^*_2Na^-$	B3LYP	6-311G**	4.0657	0.0060	−0.0860	−0.0870	0.1730	B
$Cp^*_2Na_3^+$	B3LYP	6-311G**	3.6969	0.0060	−0.0782	−0.0791	0.1573	A
$Cp^*_2Na_3^+$	B3LYP	6-311G**	3.6915	0.0051	−0.0781	−0.0790	0.1571	B
$Cp^*_2Na^-$	RHF	6-31G**	3.4629	0.0041	−0.0734	−0.0740	0.1474	A
$Cp^*_2Na^-$	RHF	6-31G**	3.4550	0.0049	−0.0732	−0.0739	0.1470	B
$Cp^*_2Na_3^+$	RHF	6-31G**	3.6261	0.0031	−0.0769	−0.0774	0.1543	A
$Cp^*_2Na_3^+$	RHF	6-31G**	3.6142	0.0037	−0.0766	−0.0772	0.1538	B
$Cp^*_2Na^-$	RHF	6-311G**	4.1778	0.0055	−0.0884	−0.0894	0.1778	A
$Cp^*_2Na^-$	RHF	6-311G**	4.1332	0.0060	−0.0874	−0.0885	0.1759	B
$Cp^*_2Na_3^+$	RHF	6-311G**	3.8237	0.0048	−0.0810	−0.0818	0.1627	A
$Cp^*_2Na_3^+$	RHF	6-311G**	3.8192	0.0051	−0.0809	−0.0817	0.1625	B

[a] Calculated EFG tensors were converted from atomic units (au) to MHz by multiplying the largest component of the EFG tensor V_{33} by $(eQ/h)(9.7177 \times 10^{21}\ \mathrm{V\ m^{-2}})$, where $Q(^{23}\mathrm{Na}) = 1.0 \times 10^{-29}\ \mathrm{m^2}$ and $e = 1.602 \times 10^{-19}$ C. [b] A represents the eclipsed structure, and B represents the structure with Cp* rings rotated 13.89°.

TABLE 5: Theoretical ^{23}Na Chemical Shift Tensors in CpNa

molecule	method	basis set	δ_{11} (ppm)	δ_{22} (ppm)	δ_{33} (ppm)	δ_{iso} (ppm)	σ_{iso} (ppm)	Ω (ppm)	κ
CpNa	exptl					−57.5(3)		12.5(3.0)	1.0
Cp_2Na^-	B3LYP	6-31G**	−77.16	−77.36	−89.16	−81.23	633.03	12.01	0.97
$Cp_2Na_3^+$	B3LYP	6-31G**	−90.82	−91.81	−91.95	−91.53	643.33	1.12	−0.76
Cp_2Na^-	B3LYP	6-311G**	−59.45	−59.68	−78.70	−65.95	626.45	19.25	0.98
$Cp_2Na_3^+$	B3LYP	6-311G**	−66.96	−67.10	−79.95	−71.34	631.84	12.99	0.98
Cp_2Na^-	RHF	6-31G**	−59.01	−59.15	−69.57	−62.57	641.61	10.56	0.97
$Cp_2Na_3^+$	RHF	6-31G**	−59.70	−59.82	−69.25	−62.92	641.96	9.55	0.98
Cp_2Na^-	RHF	6-311G**	−54.25	−54.41	−67.85	−58.84	638.05	13.60	0.98
$Cp_2Na_3^+$	RHF	6-311G**	−56.59	−56.73	−67.54	−60.29	639.50	10.95	0.97

somewhat more divergence is observed in the corresponding B3LYP calculations. Using the smaller 6-31G** basis set and the $Cp^*_2Na^-$ cluster, fairly accurate values for Ω and κ are calculated by both RHF and B3LYP methods. The eclipsed and partially eclipsed structures of Cp*Na have almost identical chemical shielding tensors. The orientations of the ^{23}Na EFG

TABLE 6: Theoretical ^{23}Na Chemical Shift Tensors in Cp*Na

molecule	method	basis set	δ_{11} (ppm)	δ_{22} (ppm)	δ_{33} (ppm)	δ_{iso} (ppm)	σ_{iso} (ppm)	Ω (ppm)	κ	geometry[a]
Cp*Na	exptl					−61.9(2)		12.0(3.0)	1.0	
$Cp^*_2Na^-$	B3LYP	6-31G**	−80.44	−81.05	−93.14	−84.88	636.68	12.70	0.90	A
$Cp^*_2Na_3^+$	B3LYP	6-31G**	−81.79	−82.22	−92.59	−85.53	637.34	10.80	0.92	A
$Cp^*_2Na^-$	B3LYP	6-311G**	−69.74	−70.25	−76.90	−72.30	632.80	7.16	0.86	A
$Cp^*_2Na_3^+$	B3LYP	6-311G**	−75.95	−76.37	−77.70	−76.67	637.18	1.75	0.53	A
$Cp^*_2Na^-$	RHF	6-31G**	−61.88	−62.27	−65.30	−63.15	642.69	13.02	0.94	A
$Cp^*_2Na_3^+$	RHF	6-31G**	−54.41	−54.70	−70.57	−59.89	638.93	16.16	0.96	A
$Cp^*_2Na^-$	RHF	6-311G**	−60.18	−60.66	−65.57	−62.14	641.35	5.39	0.82	A
$Cp^*_2Na_3^+$	RHF	6-311G**	−61.70	−62.09	−65.11	−62.97	642.18	3.42	0.77	A
$Cp^*_2Na_3^+$	RHF	6-311G**	−60.24	−60.68	−65.65	−62.19	641.41	5.41	0.84	B

[a] A represents the eclipsed structure, and B represents the structure with Cp* rings rotated 13.89°.

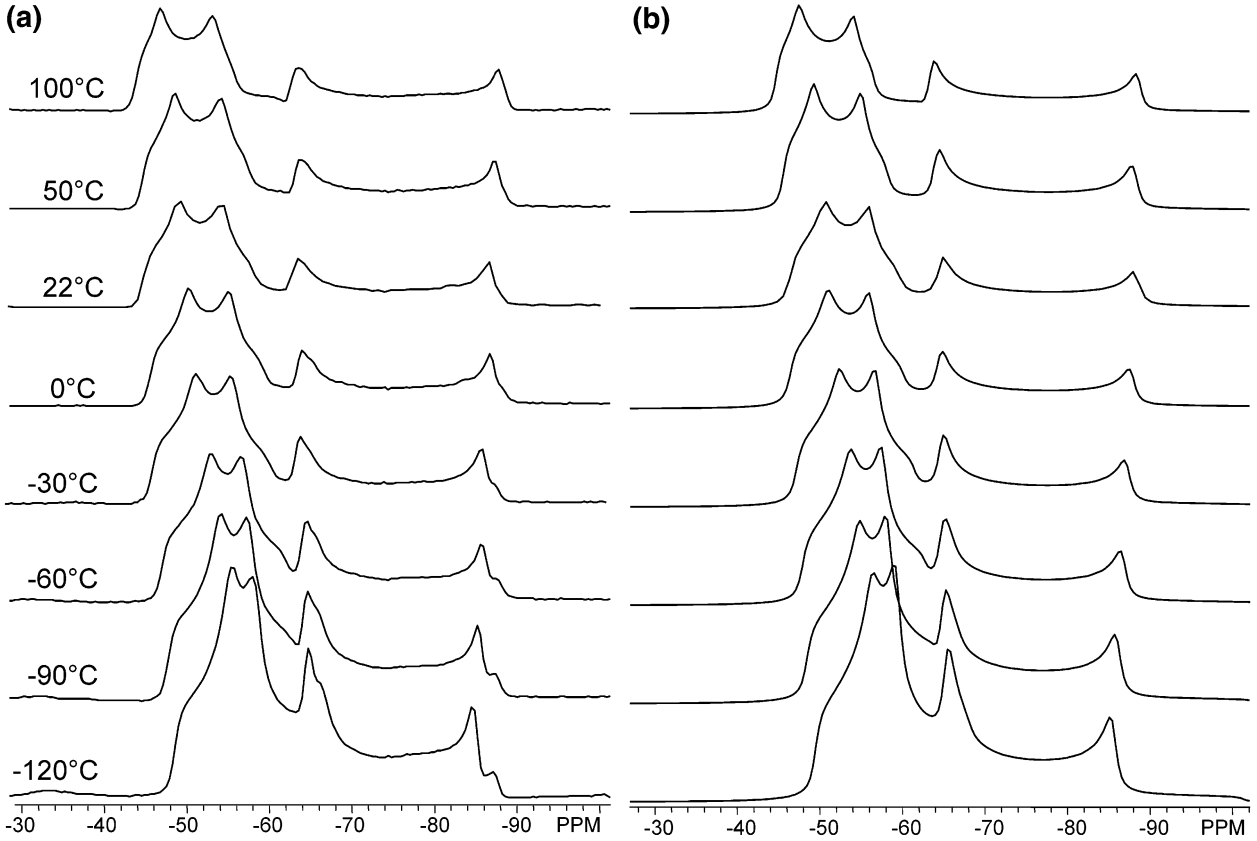

Figure 10. (a) Experimental and (b) simulated variable-temperature ^{23}Na MAS NMR spectra of a mixture of CpNa·THF and CpNa acquired with $\nu_{rot} = 9.0$ kHz.

and CS tensors are determined from the ab initio calculations and are coincident at all levels of theory. The tensors conform to the symmetry of the cluster, with the largest unique components of the tensors (V_{33} and δ_{33}) directed along the C_5 axis of the molecule (Figure 12a). The intermediate and smallest components of the tensors have similar magnitudes and are aligned along C_2 axes of the clusters, parallel to the plane of the Cp′ rings.

Carbon Chemical Shielding. The carbon chemical shielding calculations for CpNa and Cp*Na are shown in Tables 7 and 8, respectively. The trends for both compounds are very similar. The span and isotropic chemical shifts for the compounds are very insensitive to changes in the sodocene cluster size. On the other hand, the skew becomes more positive as the cluster size is increased. The calculations very closely predict the isotropic chemical shift of the compounds at all levels of theory; however, the span is overestimated for all molecules and the skew is not close to the experimentally determined value of $\kappa \approx +1.0$ (i.e., $\delta_{11} \approx \delta_{22}$).

The apparent inaccuracy of the calculation of the span and skew stems from the rapid rotation of the Cp′ rings, which is unaccounted for in calculations on the static molecule using the Gaussian 98 software. Calculations therefore yield three distinct carbon shielding tensor components that could likely only be measured experimentally at very low temperatures.[62] Due to the rotation of the Cp′ rings, the aromatic carbon sites undergo rapid chemical exchange, and the effects of the δ_{11} and δ_{22} components on the ^{13}C static spectrum are averaged. This chemical exchange was modeled using a semiclassical exchange formalism[26] implemented within a simple C++ program.[61] Initial chemical shielding tensor principal components were taken from the B3LYP/6-311G** calculation on $Cp^*_2Na_3^+$, which has the smallest calculated span. Using the carbon chemical shift tensor orientations where δ_{33} is perpendicular to the Cp* ring plane and δ_{11} is directed along the Cp-Me bond, the Euler angles for a five site exchange are $\alpha = 0$, $2\pi/5$, $4\pi/5$, $6\pi/5$, $8\pi/5$; $\beta = 0$ for all; $\gamma = 0$ for all. This corresponds to rotation of the orthogonal δ_{11} and δ_{22} components

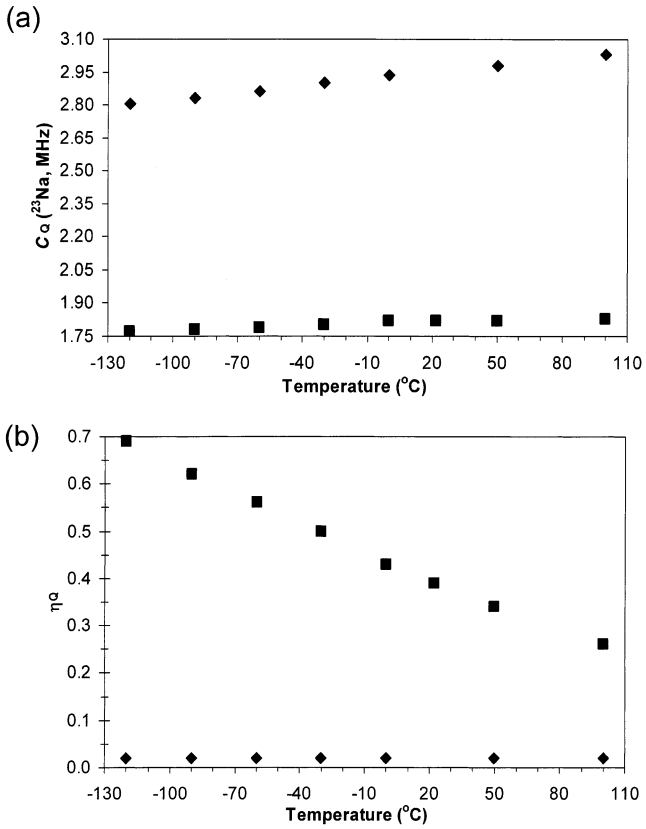

Figure 11. Plot of the variation of the (a) ^{23}Na C_Q and (b) η_Q for (◆) CpNa and (■) CpNa·THF, with temperature.

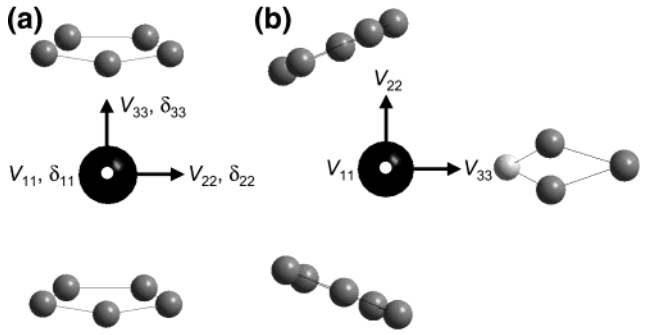

Figure 12. (a) Electric field gradient and chemical shift tensor representations of CpNa, where V_{33}, the largest component of the EFG tensor is coincident with δ_{33}, the largest component of the CS tensor. V_{11} and δ_{11} are perpendicular to the plane of the page. (b) Electric field gradient tensor representation of CpNa·THF.

about a 5-fold axis in 72° increments, leaving δ_{33} pointing in the direction of the axis of rotation. The rate of the tensor component exchange was varied from 0 (static) to greater than 25 kHz. Above 25 kHz, δ_{11} and δ_{22} exchange at a fast enough rate that an axially symmetric powder pattern results, and the shape of the theoretical spectrum matches the shape of the experimental spectrum extremely well (Figure 13), with only a slight overestimation of the span. For all of the calculations, an axially symmetric $\kappa = 1.0$ is predicted at the fast exchange limit, though the span is consistently overestimated from what appears to be overestimation of the δ_{33} component. The averages of the theoretically calculated δ_{11} and δ_{22} components are in good agreement with experimental values. It is apparent from the combination of experimentally derived carbon shielding tensors, ab initio calculations, and semiclassical exchange formalism that rotation of the Cp′ rings is occurring at a very high rate in the solid state at room temperature.

Theoretical Interpretation of Temperature-Dependent Sodocene Dynamics. Here we present results of ab initio calculations, in the hope that the unusual changes in quadrupolar parameters with temperature can be rationalized. The most obvious form of dynamic motion in these molecules is rotation of the Cp′ rings. RHF/6-311G** EFG calculations, in which the dihedral angles between the Cp′ rings were adjusted, were performed on isolated Cp_2Na^- and $Cp^*_2Na_3^+$ clusters, since these calculations reproduce the exprimental C_Q values most accurately. Rotations of the Cp′ rings have minuscule effects on the values of C_Q and the SCF energies at all levels of theory (Figure 14). The rotation of the rings results in a variation of C_Q by only 0.0015 MHz. The rotational barriers for Cp_2Na^- and $Cp^*_2Na_3^+$ are calculated to be 1.62×10^{-2} and 3.09 kJ mol^{-1}, respectively, further suggesting that the Cp′ rings undergo free rotation at ambient temperatures. In these isolated clusters, the SCF energy is at a minimum in the staggered conformation for both compounds, contrary to the solid-state structure.

Since our experimental results indicate that the values of the principal components of the EFG tensor seem to be related to the inter-ring distance, the effect of altering the Cp_{cent}−Na distances was examined. Both compounds show considerable increases in the values of C_Q as the Cp_{cent}−Na distance decreases (Figure 15). $Cp^*_2Na_3^+$ shows a greater variation in the C_Q as the distance is changed than does Cp_2Na^-. From Figure 15, the $Cp^*_2Na_3^+$ C_Q has a linear relationship with the Cp*−Na length, such that as the distance increases, C_Q decreases. Unlike $Cp^*_2Na_3^+$, the slope of the C_Q−bond length plot for Cp_2Na^- increases in magnitude (becomes more negative) as the Cp−Na distance is increased. The SCF energy for both compounds is at a minimum at ca. 2.457 Å for Cp_2Na^- and ca. 2.3557 Å for $Cp^*_2Na_3^+$. These values are distinct from the solid-state Cp'_{cent}−Na distances of 2.357 and 2.3057 Å for CpNa and Cp*Na, respectively.

It is of interest to determine what causes the increase in the magnitude of the value of C_Q as the Cp′−Na distance is reduced in sodocenes, as this will lend insight into the relationship between measured NMR parameters, temperature and sodocene structure. The electric field gradient can be calculated at a site M centered at $s_0(0,0,0)$. Assume there are n point charges of value u_i located at positions $s_i(x_i,y_i,z_i)$. An electric field gradient will be produced at s_0, which is given by the tensor

$$\bar{\mathbf{V}} = \begin{pmatrix} \sum U_{xx}^{(i)} & \sum U_{xy}^{(i)} & \sum U_{xz}^{(i)} \\ \sum U_{xy}^{(i)} & \sum U_{yy}^{(i)} & \sum U_{yz}^{(i)} \\ \sum U_{xz}^{(i)} & \sum U_{yz}^{(i)} & \sum U_{zz}^{(i)} \end{pmatrix}$$

where $U_{xx}^{(i)} = u_i r_i^{-5} (3x_i^2 - r_i^2)$, etc.; $U_{xy}^{(i)} = 3u_i r_i^{-5} x_i y_i$, etc.; and $r_i = (x_i^2 + y_i^2 + z_i^2)^{1/2}$ and the trace of $\bar{\mathbf{V}} = 0$.[75]

On a simple spreadsheet program, three CpNa geometries were investigated with varying sets of atomic point charges obtained from Mulliken population analysis within the Gaussian 98 software. It became apparent, after testing a series of different point charges, that the V_{33} component of the calculated EFG tensors is not very sensitive to subtle changes in charge on the aromatic Cp carbon atoms resulting from geometrical changes in the molecule. However, the distance of the aromatic carbon atoms from the central metal atom is paramount in determining the magnitude of C_Q. Our calculations reveal that, as the inter-ring distance is compressed from the equilibrium geometry, the magnitude of V_{33} (and therefore C_Q) increases. Conversely, as the rings are separated, the magnitude of V_{33} is observed to decrease. This trend is observed regardless of the set of point

TABLE 7: Theoretical Carbon Chemical Shift Tensors in CpNa

molecule	method	basis set	δ_{11} (ppm)	δ_{22} (ppm)	δ_{33} (ppm)	δ_{iso} (ppm)	σ_{iso} (ppm)	Ω (ppm)	κ	$(\delta_{11}+\delta_{22})/2$ (ppm)[a]	av Ω (ppm)[b]
CpNa	exptl		141.0	138.8	33.8	104.5		107.1	0.96		
Cp_2Na^-	B3LYP	6-31G**	175.58	111.22	24.62	103.81	93.52	150.96	0.15	143.40	118.78
$Cp_2Na_3^+$	B3LYP	6-31G**	180.55	117.51	21.77	106.61	90.72	158.78	0.21	149.03	127.26
Cp_2Na^-	B3LYP	6-311G**	181.83	101.87	10.86	98.19	76.58	170.98	0.07	141.85	131.00
$Cp_2Na_3^+$	B3LYP	6-311G**	183.32	114.19	8.57	102.03	72.74	174.76	0.21	148.76	140.19
Cp_2Na^-	RHF	6-31G**	177.02	106.11	10.68	97.94	99.69	166.34	0.15	141.57	130.88
$Cp_2Na_3^+$	RHF	6-31G**	178.61	111.09	7.92	99.21	98.42	170.70	0.21	144.85	136.94
Cp_2Na^-	RHF	6-311G**	181.34	99.16	0.33	93.61	85.82	181.00	0.09	140.25	139.92
$Cp_2Na_3^+$	RHF	6-311G**	181.06	109.79	-1.83	96.34	83.09	182.89	0.22	145.43	147.26

[a] Average of δ_{11} and δ_{22} resulting from chemical exchange of these components. [b] Average chemical shift span resulting from chemical exchange.

TABLE 8: Theoretical Carbon Chemical Shift Tensors in Cp*Na

molecule	method	basis set	δ_{11} (ppm)	δ_{22} (ppm)	δ_{33} (ppm)	δ_{iso} (ppm)	σ_{iso} (ppm)	Ω (ppm)	κ	$(\delta_{11}+\delta_{22})/2$ (ppm)[a]	av Ω (ppm)[b]
Cp*Na	exptl		139.8	137.9	35.9	104.6		103.9	0.96		
$Cp^*_2Na^-$	B3LYP	6-31G**	171.242	109.603	37.481	106.109	91.213	133.761	0.078	140.423	102.942
$Cp^*_2Na_3^+$	B3LYP	6-31G**	173.030	120.589	37.085	110.235	87.087	135.945	0.228	146.810	109.725
$Cp^*_2Na^-$	B3LYP	6-311G**	172.112	100.627	23.103	98.614	76.153	149.009	0.041	136.370	113.267
$Cp^*_2Na_3^+$	B3LYP	6-311G**	172.260	113.648	23.822	103.243	71.524	148.437	0.210	142.954	119.132
$Cp^*_2Na^-$	RHF	6-31G**	171.477	101.614	20.640	97.910	99.712	150.837	0.074	136.546	115.906
$Cp^*_2Na_3^+$	RHF	6-31G**	170.416	112.128	19.701	100.748	96.874	150.715	0.227	141.272	121.571
$Cp^*_2Na^-$	RHF	6-311G**	171.956	96.075	10.168	92.733	86.697	161.788	0.062	134.015	123.847
$Cp^*_2Na_3^+$	RHF	6-311G**	171.028	107.962	10.167	96.386	83.045	160.862	0.216	139.495	129.328

[a] Average of δ_{11} and δ_{22} resulting from chemical exchange of these components. [b] Average chemical shift span resulting from chemical exchange.

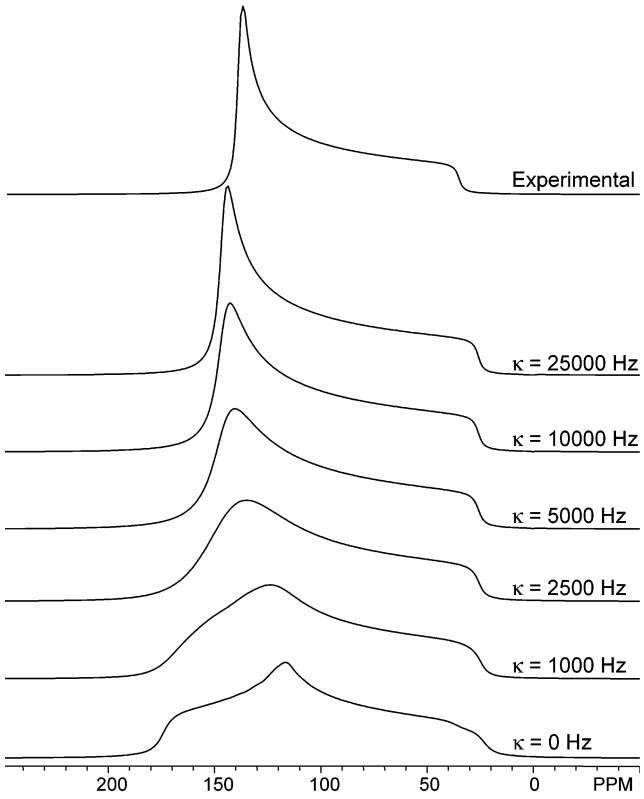

Figure 13. Theoretical (B3LYP/6-31G**) ^{13}C static NMR spectra of Cp*Na in which the smallest (δ_{11}) and intermediate (δ_{22}) components of the ^{13}C chemical shift tensor are exchanged.

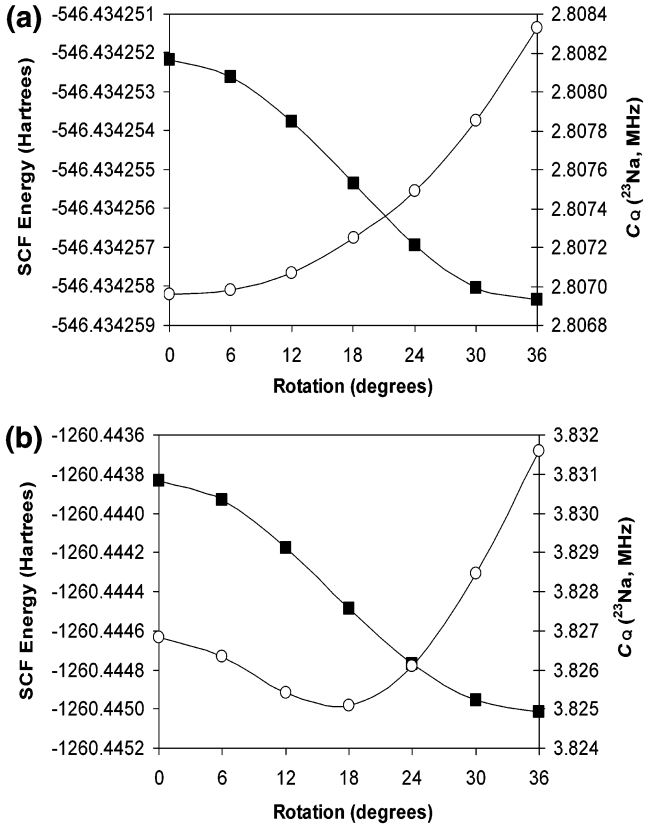

Figure 14. Theoretical (RHF/6-311G**) relationship between rotation of the Cp′ rings (0° = eclipsed) and the (○) ^{23}Na C_Q and (■) SCF energy for (a) Cp_2Na^- and (b) $Cp^*_2Na_3^+$.

charges used on the aromatic Cp carbons and protons and is in agreement with Gaussian 98 calculations.

Ab Initio Calculations of the ^{23}Na EFG Tensor in CpNa·THF. Calculations were conducted upon the geometry optimized clusters Cp_2Na^-·THF and $Cp_2Na_3^+$·THF. The majority of the calculations (Table 9), notably with the larger 6-311G** basis set, are in relatively poor agreement with the experimentally measured values and do not even predict the qualitative difference in EFG tensor parameters between CpNa and CpNa·THF clusters. This stresses the need for a reasonable solid-state structure on which to perform calculations of NMR interaction tensors. However, one interesting feature that all of the calculations share is the common orientation of the EFG tensor

TABLE 9: Theoretical ^{23}Na Electric Field Gradient Tensors in CpNa·THF

molecule	method	basis set	$\lvert C_Q \rvert$ (MHz)	η_Q	V_{11} (au)	V_{22} (au)	V_{33} (au)
CpNa·THF	exptl		1.82	0.34			
$Cp_2Na\cdot THF^-$	B3LYP	6-31G**	1.637	0.753	0.009	0.061	−0.070
$Cp_2Na_3\cdot THF^+$	B3LYP	6-31G**	2.014	0.722	−0.012	−0.074	0.086
$Cp_2Na\cdot THF^-$	B3LYP	6-311G**	2.764	0.480	0.031	0.087	−0.118
$Cp_2Na_3\cdot THF^+$	B3LYP	6-311G**	2.950	0.944	−0.004	−0.122	0.126
$Cp_2Na\cdot THF^-$	RHF	6-31G**	2.164	0.223	0.036	0.056	−0.092
$Cp_2Na_3\cdot THF^+$	RHF	6-31G**	2.280	0.615	0.019	0.078	−0.097
$Cp_2Na\cdot THF^-$	RHF	6-311G**	2.894	0.421	0.036	0.087	−0.123
$Cp_2Na_3\cdot THF^+$	RHF	6-311G**	2.897	0.927	0.005	0.119	−0.123

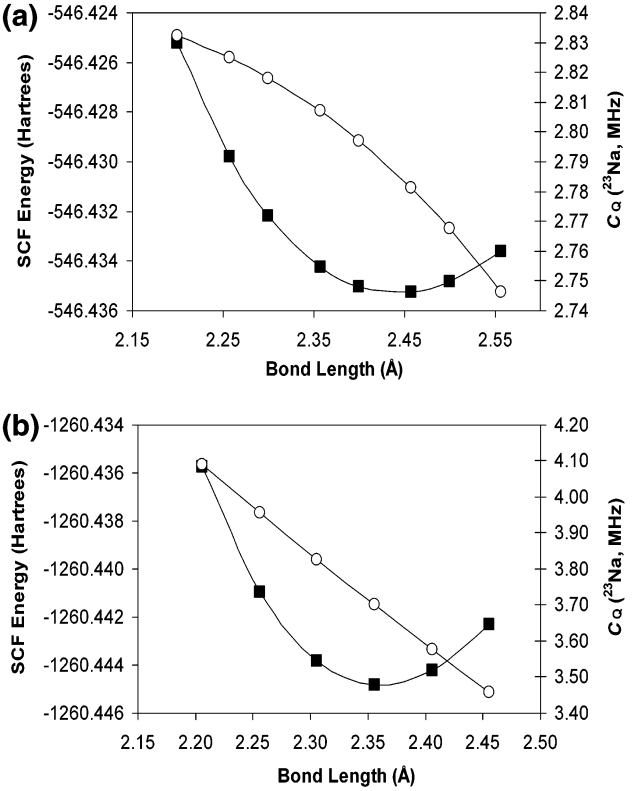

Figure 15. Theoretical (RHF/6-311G**) relationship between the Cp'_{cent}−Na bond length and the (○) ^{23}Na C_Q and (■) SCF energy for Cp_2Na^- (2.357Å = crystal structure) and (b) $Cp^*_2Na_3^+$ (2.3057 Å = crystal structure).

(Figure 12b). In CpNa·THF, the V_{33} component is directed toward the oxygen atom of the THF molecule, and V_{22} is directed toward the Cp ring. If these predicted EFG tensor orientations are at all similar to those of the solid-state structure (i.e., V_{33} should still be oriented in the direction of the coordinated THF), the unusual temperature behavior observed in VT ^{23}Na MAS NMR experiments can be easily rationalized. If compression of the unit cell along the zigzagging, bent CpNa chain occurs, V_{33} would not be influenced and C_Q would remain constant. However, V_{22} would change significantly as the Cp_{cent}−Na−Cp_{cent} angle changes, resulting in a constant temperature-dependent change in η_Q. Accurate theoretical treatment of the ^{23}Na EFG and CS tensors in CpNa.THF and related analogues, and the treatment of the unusual temperature-dependence of these tensors, are beyond the scope of this manuscript and will be the subject of a forthcoming paper.

Conclusions

Solid-state ^{23}Na NMR has been shown to be an excellent probe of the electronic environment of the sodium atom in sodium metallocenes. The ^{23}Na EFG tensor is very sensitive to changes in both the geometry and structure of these molecules. Very small changes in the chemistry of sodocenes, which arise from substitution of the Cp ring, cause changes in the magnitude of the quadrupolar interaction. In addition, bending of the sodocene chains, resulting from ligand coordination to the sodium metal, causes substantial changes to the asymmetry parameter. The quadrupolar interaction is also an excellent probe of molecular dynamics in sodocenes, with variable-temperature ^{23}Na NMR experiments demonstrating that variation of temperature can cause significant changes in sodocene structure. The increase in the C_Q with increasing temperature has been shown, with the aid of ab initio calculations, to result from a decrease in the metal-ring distances in these compounds. In addition, the lower C_Q, which was previously measured for the less symmetric CpNa-TMEDA compound, was determined to result predominantly from the dramatically larger Cp−Na distance in this molecule.

Rare instances of sodium CSA are observed for all four metallocene complexes. The shape of the static powder patterns, which are broad due to a large quadrupolar interaction, have been shown to be dependent on the strength of the rf field. A low rf field and short pulse widths are required for uniform excitation of the powder pattern. Uniform excitation is essential for the accurate extraction of CS tensor data from spectra that are complicated by the combined effects of EFG and CSA.

Ab initio calculations have been used to study sodium EFG and CS tensors in sodocenes. Calculated C_Q and η_Q are in relatively good agreement with experimental parameters. Anisotropic sodium chemical shielding is predicted at all levels of theory, in qualitative agreement with experiment. The largest component of the EFG tensor V_{33} is directed into the plane of the rings, along the pseudo-C_5 axis of the molecules. Free rotation of the Cp′ rings has been shown to have little effect on the C_Q. However, the C_Q proves to be very sensitive to changes in the inter-ring distance of the sodocenes and is used to describe the strange experimental C_Q temperature dependence in these compounds. Simulation of experimental ^{13}C powder patterns and comparison with ab initio data via a semiclassical exchange model demonstrates that the experimentally observed powder pattern results from rapid averaging of the δ_{11} and δ_{22} components of the aromatic carbon chemical shielding tensors. Experimental NMR data and preliminary calculations of EFG tensors in CpNa·THF assist in understanding the variable-temperature behavior of these molecules.

The comprehensive experimental and theoretical characterization of ^{23}Na and ^{13}C NMR interaction tensors reveals much about molecular structure and dynamics in these polymeric metallocenes. Relatively simple solid-state NMR experiments and corresponding spectral simulations and theoretical calculations clearly provide an efficient means of gauging the purity of the sample, the local electronic environments of the quadrupolar nuclei, as well as the temperature-dependent motion of the sodium atoms and cyclopentadienyl rings. We believe the

application of solid-state NMR methods to the study of polymeric metallocenes is of utmost importance; given that there are many polymeric metallocene systems used as starting materials in a variety of synthetic procedures that can rapidly be checked for purity and quality, there are many solid-state polymeric systems that cannot be studied using X-ray methods due to their amorphous or semicrystalline nature, and there are a large number of fascinating structural motifs for metallocenes (with as of yet unknown molecular dynamics) that have not yet been characterized.

Acknowledgment. We wish to thank Professor Doug Stephan (University of Windsor) for use of his gloveboxes for sample preparation and Dr. Silke Courtenay (Queens University) for assistance in synthesis and sample preparation. We also thank Professor Charles Macdonald (University of Windsor) for advice regarding synthesis and chemistry of polymeric metallocenes, as well as for a thorough proofreading of this manuscript. We gratefully acknowledge Ms. Siri Schauff for her initial work on this project and Mr. Cory Widdifield for completing some of the spectral simulations and error analysis. We are also grateful to Prof. Clare Grey and Mr. Peter Chupas (State University of New York at Stony Brook) for helpful discussions regarding the relationship of solid-state structure and temperature and to Prof. Robert E. Dinnebier (Max Planck Institute) for providing a crystallographic data file for Cp*Na. R.W.S. is grateful to Imperial Oil for an Imperial Oil Research Grant, and the National Science and Engineering Research Council (NSERC) of Canada for funds in the form of an Operation Grant and Collaborative Research and Development Grant. R.W.S. also thanks the Canadian Foundation for Innovation and the Ontario Innovation Trust for funding for the new solid-state NMR facility at the University of Windsor. M.J.W. thanks the Centre for Catalysis and Materials Research (CCMR) at the University of Windsor for a Summer Research Scholarship.

Supporting Information Available: Tables of VT NMR parameters, theoretical dynamical EFG parameters, and Cartesian coordinates used for ab initio calculations. This material is available free of charge via the Internet at http://pubs.acs.org.

References and Notes

(1) Jutzi, P.; Burford, N. *Chem. Rev.* **1999**, *99*, 969.
(2) Harder, S. *Coord. Chem. Rev.* **1998**, *176*, 17.
(3) Jutzi, P.; Leffers, W.; Hampel, B.; Pohl, S.; Saak, W. *Angew. Chem., Int. Ed. Engl.* **1987**, *26*, 583.
(4) Evans, W. J.; Boyle, T. J.; Ziller, J. W. *Organometallics* **1992**, *11*, 3903.
(5) Harvey, M. J.; Hanusa, T. P.; Pink, M. *J. Chem. Soc., Dalton Trans.* **2001**, 1128.
(6) Rietveld, H. M. *Acta Crystallogr.* **1967**, *22*, 151.
(7) Rietveld, H. M. *J. Appl. Crystallogr.* **1969**, *2*, 65.
(8) Dinnebier, R. E.; Behrens, U.; Olbrich, F. *Organometallics* **1997**, *16*, 3855.
(9) Dinnebier, R. E.; Olbrich, F.; van Smaalen, S.; Stephens, P. W. *Acta Crystallogr., Sect. B: Struct. Sci.* **1997**, *B53*, 153.
(10) Dinnebier, R. E.; Olbrich, F.; Bendele, G. M. *Acta Crystallogr., Sect. C: Cryst. Struct. Commun.* **1997**, *53*, 699.
(11) Dinnebier, R. E.; Schneider, M.; van Smaalen, S.; Olbrich, F.; Behrens, U. *Acta Crystallogr., Sect. B: Struct. Sci.* **1999**, *55*, 35.
(12) Tedesco, C.; Dinnebier, R. E.; Olbrich, F.; van Smaalen, S. *Acta Crystallogr., Sect. B: Struct. Sci.* **2001**, *57*, 673.
(13) Janiak, C.; Schumann, H.; Stader, C.; Wrackmeyer, B.; Zuckerman, J. J. *Chem. Ber./Recl.* **1988**, *121*, 1745.
(14) Wrackmeyer, B.; Kupce, E.; Kehr, G.; Sebald, A. *Magn. Reson. Chem.* **1992**, *30*, 964.
(15) Armstrong, D. R.; Duer, M. J.; Davidson, M. G.; Moncrieff, D.; Russell, C. A.; Stourton, C.; Steiner, A.; Stalke, D.; Wright, D. S. *Organometallics* **1997**, *16*, 3340.
(16) Keates, J. M.; Lawless, G. A. *Organometallics* **1997**, *16*, 2842.
(17) Spiess, H. W.; Haas, H.; Hartmann, H. *J. Chem. Phys.* **1969**, *50*, 3057.
(18) Johnels, D.; Boman, A.; Edlund, U. *Magn. Reson. Chem.* **1998**, *36*, S151.
(19) Pietrass, T.; Burkert, P. K. *Inorg. Chim. Acta* **1993**, *207*, 253.
(20) Schurko, R. W.; Hung, I.; Macdonald, C. L. B.; Cowley, A. H. *J. Am. Chem. Soc.* **2002**, *124*, 13204.
(21) Schurko, R. W.; Hung, I.; Schauff, S.; Macdonald, C. L. B.; Cowley, A. H. *J. Phys. Chem. A* **2002**, *106*, 10096.
(22) Pyykko, P.; Sadlej, A. J. *Chem. Phys. Lett.* **1994**, *227*, 221.
(23) Klosters, G.; Jansen, M. *Solid State Nucl. Magn. Reson.* **2000**, *16*, 279.
(24) Akitt, J. W. In *Multinuclear NMR*; Mason, J., Ed.; Plenum Press: New York, 1987; p 193.
(25) Terskikh, V. V.; Lapina, O. B.; Bondareva, V. M. *PCCP Phys. Chem. Chem. Phys.* **2000**, *2*, 2441.
(26) Mehring, M. *Principles of High-Resolution NMR in Solids*; Springer-Verlag: New York, 1983.
(27) Mason, J. *Solid State Nucl. Magn. Reson.* **1993**, *2*, 285.
(28) Power, W. P.; Wasylishen, R. E.; Mooibroek, S.; Pettitt, B. A.; Danchura, W. *J. Phys. Chem.* **1990**, *94*, 591.
(29) Ford, W. T. *J. Organomet. Chem.* **1971**, *32*, 27.
(30) Fischer, P.; Stadelhofer, J.; Weidlein, J. *J. Organomet. Chem.* **1976**, *116*, 65.
(31) Ito, T.; Yoden, T. *Bull. Chem. Soc. Jpn.* **1993**, *66*, 2365.
(32) McLean, S.; Haynes, P. *Can. J. Chem.* **1963**, *41*, 1231.
(33) Alderman, D. W.; Solum, M. S.; Grant, D. M. *J. Chem. Phys.* **1986**, *84*, 3717.
(34) Eden, M.; Levitt, M. H. *J. Magn. Reson.* **1998**, *132*, 220.
(35) Code is available at http://www.netlib.org/lapack.
(36) Frisch, M. J.; Trucks, G. W.; Schlegel, H. B.; Scuseria, G. E.; Robb, M. A.; Cheeseman, J. R.; Zakrzewski, V. G.; Montgomery, J. A., Jr.; Stratmann, R. E.; Burant, J. C.; Dapprich, S.; Millam, J. M.; Daniels, A. D.; Kudin, K. N.; Strain, M. C.; Farkas, O.; Tomasi, J.; Barone, V.; Cossi, M.; Cammi, R.; Mennucci, B.; Pomelli, C.; Adamo, C.; Clifford, S.; Ochterski, J.; Petersson, G. A.; Ayala, P. Y.; Cui, Q.; Morokuma, K.; Malick, D. K.; Rabuck, A. D.; Raghavachari, K.; Foresman, J. B.; Cioslowski, J.; Ortiz, J. V.; Baboul, A. G.; Stefanov, B. B.; Liu, G.; Liashenko, A.; Piskorz, P.; Komaromi, I.; Gomperts, R.; Martin, R. L.; Fox, D. J.; Keith, T.; Al-Laham, M. A.; Peng, C. Y.; Nanayakkara, A.; Challacombe, M.; Gill, P. M. W.; Johnson, B.; Chen, W.; Wong, M. W.; Andres, J. L.; Gonzalez, C.; Head-Gordon, M.; Replogle, E. S.; Pople, J. A. *Gaussian 98*, revision A.9; Gaussian, Inc.: Pittsburgh, PA, 1998.
(37) Becke, A. D. *J. Chem. Phys.* **1993**, *98*, 5648.
(38) Lee, C. T.; Yang, W. T.; Parr, R. G. *Phys. Rev. B* **1988**, *37*, 785.
(39) Bryant, P. L.; Harwell, C. R.; Wu, K.; Fronczek, F. R.; Hall, R. W.; Butler, L. G. *J. Phys. Chem. A* **1999**, *103*, 5246.
(40) Brown, R. D.; Headgordon, M. P. *Mol. Phys.* **1987**, *61*, 1183.
(41) Cummins, P. L.; Bacskay, G. B.; Hush, N. S. *Mol. Phys.* **1987**, *62*, 193.
(42) Wolinski, K.; Hinton, J. F.; Pulay, P. *J. Am. Chem. Soc.* **1990**, *112*, 8251.
(43) Samoson, A.; Lippmaa, E. *J. Magn. Reson.* **1988**, *79*, 255.
(44) Nielsen, N. C.; Bildsoe, H.; Jakobsen, H. J. *J. Magn. Reson.* **1992**, *98*, 665.
(45) Koller, H.; Engelhardt, G.; Kentgens, A. P. M.; Sauer, J. *J. Phys. Chem.* **1994**, *98*, 1544.
(46) Akitt, J. W.; McDonald, W. S. *J. Magn. Reson.* **1984**, *58*, 401.
(47) Aoyagi, T.; Shearer, H. M. M.; Wade, K.; Whitehead, G. *J. Organomet. Chem.* **1979**, *175*, 21.
(48) Schreckenbach, G. *J. Chem. Phys.* **1999**, *110*, 11936.
(49) Sagnowski, S. F.; Sulek, Z.; Stachura, M.; Ogar, J. *Z. Phys. B: Condens. Mater.* **1982**, *46*, 123.
(50) Sagnowski, S. F.; Ogar, J. *Phys. Status Solidi B* **1981**, *107*, K125.
(51) Wong, A.; Wu, G. *J. Phys. Chem. A* **2000**, *104*, 11844.
(52) Man, P. P. *Phys. Rev. B* **1995**, *52*, 9148.
(53) Dumazy, Y.; Amoureux, J. P.; Fernandez, C. *Mol. Phys.* **1997**, *90*, 959.
(54) Frydman, L.; Harwood, J. S. *J. Am. Chem. Soc.* **1995**, *117*, 5367.
(55) Lucken, E. A. C. *Nuclear Quadrupole Coupling Constants*; Academic Press: New York, 1969.
(56) Das, T. P.; Hahn, E. L. *Nuclear Quadrupole Resonance Spectroscopy*; Academic Press: New York, 1958.
(57) Witschas, M.; Eckert, H.; Freiheit, H.; Putnis, A.; Korus, G.; Jansen, M. *J. Phys. Chem. A* **2001**, *105*, 6808.
(58) Wagner, M. J.; McMills, L. E. H.; Ellaboudy, A. S.; Eglin, J. L.; Dye, J. L.; Edwards, P. P.; Pyper, N. C. *J. Phys. Chem.* **1992**, *96*, 9656.
(59) Fechtelkord, M. *Solid State Nucl. Magn. Reson.* **2000**, *18*, 70.
(60) Liang, J. J.; Sherriff, B. L. *Geochim. Cosmochim. Acta* **1993**, *57*, 3885.
(61) Schurko, R. W.; Wi, S.; Frydman, L. *J. Phys. Chem. A* **2002**, *106*, 51.

(62) Orendt, A. M.; Facelli, J. C.; Jiang, Y. J.; Grant, D. M. *J. Phys. Chem. A* **1998**, *102*, 7692.
(63) Heyes, S. J.; Dobson, C. M. *J. Am. Chem. Soc.* **1991**, *113*, 463.
(64) Campbell, A. J.; Fyfe, C. A.; Maslowsky, E., Jr. *J. Am. Chem. Soc.* **1972**, *94*, 2690.
(65) Herzfeld, J.; Berger, A. E. *J. Chem. Phys.* **1980**, *73*, 6021.
(66) Wemmer, D. E.; Pines, A. *J. Am. Chem. Soc.* **1981**, *103*, 34.
(67) Wemmer, D. E.; Ruben, D. J.; Pines, A. *J. Am. Chem. Soc.* **1981**, *103*, 28.
(68) Nie, W. L.; Qian, C. T.; Chen, Y. F.; Sun, J. *Organometallics* **2001**, *20*, 5780.
(69) Leung, W. P.; Song, F. Q.; Xue, F.; Mak, T. C. W. *J. Chem. Soc., Dalton Trans.* **1997**, 4307.
(70) Herberich, G. E.; Fischer, A. *Organometallics* **1996**, *15*, 58.
(71) Zhang, S. B.; Liu, J. Z.; Wei, G. C.; Lin, G. Y.; Chen, W. Q. *Polyhedron* **1993**, *12*, 2771.
(72) Harder, S.; Prosenc, M. H.; Rief, U. *Organometallics* **1996**, *15*, 118.
(73) Aoyagi, T.; Shearer, H. M. M.; Wade, K.; Whitehead, G. *J. Chem. Soc., Chem. Commun.* **1976**, 164.
(74) Silverstein, R. M.; Webster, F. X. *Spectrometric Identification of Organic Compounds*, 6th ed.; John Wiley and Sons: New York, 1998.
(75) Knop, O. *Acta Crystallogr., Sect. A: Found. Crystallogr.* **1976**, *A32*, *Pt. 1*, 147.